MOUNTAIN-PLAINS CONSORTIUM

MPC 18-356 | Z. Song, Y. He, and Z. Liu

Implementation of Aerial LiDAR Technology to Update Highway Feature Inventory

MOUNTAIN-PLAINS CONSORTIUM REGION 8

A University Transportation Center sponsored by the U.S. Department of Transportation serving the Mountain-Plains Region. Consortium members:

Colorado State University
North Dakota State University
South Dakota State University
University of Colorado Denver
University of Denver
University of Utah
Utah State University
University of Wyoming

IMPLEMENTATION OF AERIAL LIDAR TECHNOLOGY TO UPDATE HIGHWAY FEATURE INVENTORY

Ziqi Song, Ph.D
Assistant Professor

Yi He
Graduate Research Assistant

Zhaocai Liu
Graduate Research Assistant

Department of Civil and Environmental Engineering
Utah State University

July 2018

Acknowledgements

The funds for this study were provided by the United States Department of Transportation to the Mountain-Plains Consortium (MPC) and Utah Department of Transportation (UDOT). The authors acknowledge the following individuals from UDOT on the Technical Advisory Committee for helping to guide the research:

- Lloyd Neeley
- Rukhsana Lindsey
- Michael Butler
- Jefferson Searle
- Thomas Hales
- Kevin Griffin

Disclaimer

ABSTRACT

Highway assets, including traffic signs, traffic signals, light poles, and guardrails, are important components of transportation networks. They guide, warn, and protect drivers and regulate traffic. To manage and maintain the regular operation of the highway system, state departments of transportation (DOTs) need reliable and up-to-date information about the location and condition of highway features. The focus of this project is to analyze the capability and strengths of an airborne data collection system in highway inventory data collection. A field experiment was conducted to collect both light detection and ranging (LiDAR) point cloud data and high-resolution aerial imagery data. A comprehensive introduction to highway inventory methodologies, especially airborne LiDAR technology, was provided. An ArcGIS-based algorithm was developed to analyze and process LiDAR data as well as extract desirable features from raw LiDAR point clouds. In addition, a MATLAB-based drainage grate detection algorithm was proposed to demonstrate the effectiveness and economic efficiency of the airborne data collection system. The detection results were compared with a Mandli dataset. An economic comparison between airborne LiDAR and mobile LiDAR was also provided. From the results of this project, we can conclude that airborne LiDAR technology is a promising method for road inventory data collection.

TABLE OF CONTENTS

LIST OF TABLES

LIST OF FIGURES

EXECUTIVE SUMMARY

Highway inventory plays an important role in highway management. Governments and agencies have been employing different kinds of methodologies for highway inventory. Existing methodologies include field inventory, photo/video log, integrated global positioning system (GPS)/global information system (GIS) mapping, aerial/satellite photography, terrestrial light detection and ranging (LiDAR), mobile LiDAR, and airborne LiDAR. Each has advantages and disadvantages as well as limitations in collecting road inventory data. This paper mainly focuses on the application of airborne data collection method.

Four highway sections in Utah were mapped in this experiment: one on Interstate 84 (I-84), two on Interstate 15 (I-15 north and I-15 south), and one on US-191. Both LiDAR point cloud data and high-resolution aerial imagery data were obtained. This project mainly focused on processing and analyzing the LiDAR point cloud data by using ArcGIS, but also provided an automatic road sign detection algorithm based on MATLAB for the aerial images.

A comprehensive introduction to highway inventory methodologies, especially airborne LiDAR technology, was provided to relevant departments and personnel to promote their understanding of the pros and cons of different inventory techniques. An ArcGIS-based algorithm was developed to analyze and process LiDAR data and to extract desirable features from raw LiDAR point clouds. In addition, a MATLAB-based feature extraction algorithm was also proposed to demonstrate the effectiveness and economic efficiency of the airborne data collection system.

The results showed that although small signs (e.g., speed limit signs) along highways cannot be identified successfully because of the low point density of airborne LiDAR data, other features, such as guardrails, median strips, light poles, and large signs, are very easy to detect. Also, from airborne LiDAR data, one can detect features like culverts and bridges, which cannot be detected by mobile mapping or other inventory techniques. Furthermore, airborne LiDAR data provide accurate coordinate information for the detected highway features. For aerial images, we can also extract some kind of assets based on the assets' color, shape, or other characteristics.

The findings of this research can be used as a reference for the Utah Department of Transportation (UDOT) and other state DOTs before they choose a methodology to collect highway inventory data. Also, the LiDAR-data-based and image-based road sign extraction methods may provide inspiration for future researchers to develop more effective and efficient methods for road sign detection.

1. INTRODUCTION

1.1 Problem Statement

The main focus of this research project is to evaluate the application of the airborne light detection and ranging (LiDAR) system when updating the highway inventory database. Highway assets, such as traffic signs and signals, directional signs, mile markers, streetlights, guardrails, and culverts, play a vital role in regulating traffic and guiding and warning drivers as well as pedestrians. Therefore, it is helpful for state departments of transportation (DOTs) to have up-to-date inventory data to establish the condition of the road networks within their states, prioritize reconstruction and repair work, and value their highway assets. DOTs also use road inventory data for traffic engineering studies, planning, and meeting federal data reporting requirements. Because of the importance of collecting highway inventory data, many methodologies have been proposed to gather the data. The techniques range from the simplest manual inventory method to methods that involve advanced technology, such as aerial photography and LiDAR. In the past few years, various state DOTs have conducted inventory data collection using a number of methods. Among these methods, photo/video log and integrated global positioning system (GPS) and global information system (GIS) mapping are popular because of their low initial cost and ease of operation. For example, Washington DOT has adopted photo log and integrated GPS/GIS mapping for roadway data collection. Michigan DOT has utilized the integrated GPS/GIS mapping method and field inventory, and Idaho DOT has used video log. On the other hand, mobile LiDAR and airborne LiDAR, even though they involve higher equipment costs and are relatively new technologies, are being employed by more and more state DOTs and transportation agencies.

A substantial amount of work has been done to analyze different methodologies for road inventory. For example, Khattak et al. (2000) conducted four experiments to compare the traditional manual method with the integrated GIS/GIS mapping systems. Jeyapalan (2004) developed a method to obtain the three-dimensional locations of road features with data captured from a video logging system. Landa and Prochazka (2014) compared RGB (red, green, and blue) image-based road inventory and LiDAR-based road inventory, finding that road sign detection from RGB data is much cheaper and can include color information, while more precise position and height information can be obtained from LiDAR data. They also provided a traffic sign detection method based on point clouds obtained by a mobile laser scanning system, and tested their method on a road section in Brno, Czech Republic. The results showed relatively high precision in their proposed LiDAR-based method. Jalayer et al. (2015) evaluated the capability of the photo/video log to collect geospatial highway inventory data required by the Highway Safety Manual (HSM). The authors conducted a web-based nationwide survey to analyze the advantages and disadvantages of photo and video logs, as well as a field trial that recorded the data-collected time and data-reduction time for three different types of roadway segments (rural two-lane highway, rural multilane highway, and urban and suburban arterial segments) using the photo and video logging method. Based on the survey and the trial, the authors concluded that geo-tagged photo and video log technology is one of the most economical and efficient methods for DOTs to conduct data collection.

Despite LiDAR becoming increasingly popular across the United States, and state DOTs and transportation agencies adopting LiDAR technology to deal with transportation-related applications, to date, airborne LiDAR is still not as popular as other inventory techniques because of its expensive initial investment and limitations in identifying small objects. The main purpose of this research is to analyze the advantages and disadvantages of airborne LiDAR technology in collecting and recording highway assets. Furthermore, because aerial imagery data are relatively easy to acquire when the aircraft is flying, imagery data were also collected along with the LiDAR data for a joint analysis.

1.2 Research Objectives

To achieve the goal of this research project, the following objectives were identified:

- Conduct a literature review covering the existing road inventory technologies, especially for airborne LiDAR technology;
- Carry out a field trial to collect both airborne LiDAR data and high-resolution aerial images of four highway sections in Utah: two on Interstate 15 (I-15), one on Interstate 84 (I-84), and one on US-191;
- Develop a GIS-based algorithm to process the raw LiDAR point clouds to extract candidate highway assets, and then apply the manual recording method to assess the location and structure information of the assets;
- Propose a MATLAB-based method to process the imagery data, and detect drainage grates with high accuracy;
- Investigate the feasibility of using airborne LiDAR to supplement mobile LiDAR by identifying assets that mobile LiDAR cannot;
- Compare the pros and cons of the airborne LiDAR technology with the mobile counterpart.

1.3 Expected Contributions

Highway inventory data collection should be conducted periodically to check the completeness of road infrastructure and assets to ensure safety. This is a very costly project for most transportation agencies; not only a large number of crews are sent out for a long time, but the crews are also exposed to traffic, which is not safe. The airborne mapping technique is often more cost-effective than conventional surveying methods and has other additional values, such as no disruption to traffic and improved safety. Thus, proving that data collected through airborne mapping can also provide effective information about road assets will help state DOTs and transportation agencies save large amounts of resources on road inventory in the future. Our research project assessed an aerial mapping technology, airborne LiDAR, in highway assets detection, demonstrating that airborne LiDAR is a promising technique for relevant agencies to collect road inventory data in the future.

1.4 Outline of the Report

Section 1 has provided a brief introduction to the research. Section 2 introduces different kinds of existing technologies for road surveying. Section 3 focuses primarily on the introduction of LiDAR, especially the advantages and applications of airborne LiDAR. In Section 4, the field experiment and data collection will be presented. Section 5 develops an ArcGIS-based algorithm to analyze LiDAR data, and provides the data analysis results. Section 6 proposes an image processing method based on MATLAB to detect highway drainage grates. Section 7 concludes the report. This report is based on Yi, 2016, Yi et al., 2016, and Yi et al., 2017a, b.

2. INTRODUCTION OF ROAD SURVEYING METHODOLOGIES

Road surveying/inventory is a compilation of components and conditions of a road system. Collecting and storing roadside assets data, such as lane width, traffic sign height, location, and condition, help transportation agencies make future safety and maintenance investment decisions and provide program managers with better information for program prioritization. For example, the recently published Highway Safety Manual (HSM) (2010) has assisted many state DOTs to evaluate the highway safety performance at different construction stages and operation stages. However, some state DOTs are still in the awkward position of lacking HSM-required highway inventory data (HID). Given the importance of the information of roadside features to the management of roadways, finding effective and economic methods to enrich the inventory data system is fairly urgent.

State DOTs and local transportation agencies have employed different types of HID collection techniques, such as field inventory, photo/video log, integrated global positioning system (GPS) and global information system (GIS) mapping systems, aerial/satellite photography, terrestrial light detection and ranging (LiDAR), mobile LiDAR, and airborne LiDAR. These techniques vary in time consumption, costs, effectiveness, and accuracy. In this section, we provide a brief introduction to each of these techniques, and focus mainly on their advantages and disadvantages in the application of road inventory data collection.

Existing roadway inventory data collection methods can be roughly divided into two categories: ground-based and air- or space-based methods (Zhou et al., 2013). Based on the equipment of these systems, they can also be divided into three categories: based on GPS, based on GPS and image, and based on GPS, image, and LiDAR. The classification of existing road inventory data collection methods is given in Table 2.1.

Table 2.1 Classification of Existing Road Inventory Data Collection Methods

	GPS	**GPS and Image**	**GPS, Image and LiDAR**
Land-based	• Field Inventory • Integrated GPS/GIS Mapping Systems	• Photo/Video log	• Terrestrial LiDAR • Mobile LiDAR
Air- or Space-based		• Aerial/Satellite Photography	• Airborne LiDAR

2.1 Manual/Field Inventory

The first proposal and implementation of collecting roadway inventory data dates back to the mid-1890s (Degray and Hancock, 2002). At that time, road inventory mainly relied on manual collection, which is also known as field inventory. Typically, as shown in Figure 2.1, manual inventory needs data collectors, a vehicle, a distance measuring instrument (DMI), and paper and pencils or a laptop for collecting and recording georeference (i.e., latitude, longitude, and altitude) and descriptive (i.e., length, width, height, and condition) data (Khattak et al., 2000). Although this method is time consuming, loosely organized, and unsafe because crews are exposed to traffic and field, its capability of collecting rich and accurate data and its low initial cost still make it quite a competitive method.

As the nation's road network rapidly and continuously grew, manual collection could no longer satisfy the huge and sophisticated needs for roadway data. New technologies emerged, allowing for more efficient

data collection and recording. However, field inventory is still required and cannot be completely replaced by later technologies, as new technologies may not be able to collect data on all kinds of assets.

The advantages and disadvantages of manual inventory are summarized as follows:

Advantages

- Low equipment cost
- Minimal training requirements for personnel
- Low data reduction efforts
- Capable of collecting rich road inventory data
- Capable of collecting feature conditions

Disadvantages

- Personnel exposed to dangerous traffic environment
- Hinder the traffic to some extent
- Long collection time
- Labor intensive
- Less accuracy

Figure 2.1 Field Inventory

2.2 Photo/Video Log

Image inventory, also known as photo logging, is based on cameras taking images of a roadway at constant intervals along the road. The primary difference between the photo log and video log is that they use different recording mediums. A photo log is obtained by automatically recording pictures while the vehicle is moving along the roadway, whereas a video log records continuous images.

Equipped with a high-resolution digital camera, a GPS receiver, and an inertial navigation system (INS), the mobile photo/video logging system has been widely used for capturing roadway features in recent years. For example, approximately 27,000 miles of roadway in Tennessee were mapped by photo log

(Tao, 2000). Jeyapalan and Bhagawati (2000) used the video logging method (Figure 2.2) to collect roadside assets at a scale of 25 feet or less in order to create a geographic information system. Then in 2002, Jeyapalan and Jaselskis used video logs for their study (Jeyapalan and Jaselskis, 2002), testing three sites with video logging van-captured images: Grand Avenue, EDM baseline, and US-30. A few years later, the video logging technique was once again used by Jeyapalan, who developed a method for determining the three-dimensional (3D) locations of road features by using images obtained from a video logging system (Jeyapalan, 2004).

Compared with field inventory, most of the work of a photo/video log can be done indoors, thereby reducing potential hazards to data collection personnel. Only one or two personnel are required, and they ride inside the vehicle without direct exposure to traffic. Therefore, the photo logging method is more efficient and safer. In addition, the data collected by a photo log are more accurate and uniformly recorded, because field inventory is generally conducted by several different crews whose operating levels toward measurement equipment and degree of caution may be remarkably diverse. Thus, there tends to be more errors in field inventory.

But this method collects lots of useless information, hence, it needs large data reduction efforts. It is also not able to measure feature dimensions. Another disadvantage of a photo log or video log is that the collected data quality is subject to weather conditions.

Figure 2.2 Video Logging *Jevapalan and Bhagawati 2000)

2.3 Integrated GPS/GIS Mapping System

An integrated GPS/GIS mapping system is a commonly used technology among DOTs and transportation agencies for roadside inventory. Most integrated GPS/GIS mapping systems are also equipped with an INS, which is the backup system when GPS loses its lock due to signal obstruction so that the mapping system can obtain continuous position information (Figure 2.3).

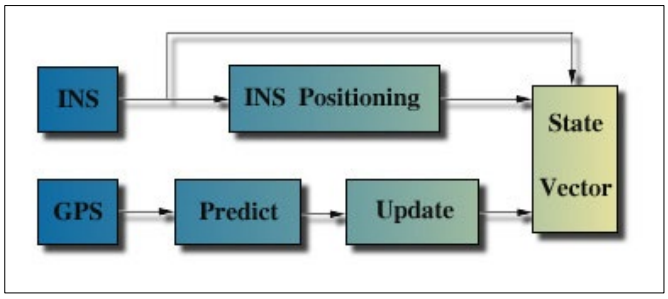

Figure 2.3 The GPS/INS Integration Procedure

(Source: http://www.lambdatech.com)

Figure 2.4 Integrated GPS/GIS Mapping

(Source: http://www.irmforestry.com/habitat-restoration-services/
restoration-management -planning/gis-mapping/
http://www.waypointtech.com/rentals/gps-mapping-systems/)

The advantages of the integrated GPS/GIS method are that it needs relatively low initial cost and low data reduction efforts, and it improves data accuracy. However, crews have to be exposed to the traffic and field during long data collection periods (Figure 2.4).

2.4 Aerial/Satellite Photography

High-resolution images taken from an aircraft or satellite can be used for analyzing road networks. Hallmark et al. (2001) tested the use of remotely sensed images with different resolution levels (2-inch resolution, 6-inch resolution, 24-inch resolution, and 1-meter resolution) on road inventory feature detection. They found that most features could be successfully identified in the 2-inch and 6-inch datasets, while only large features, such as intersections and railroad crossings, had relatively higher identification rates in the 24-inch or 1-meter datasets.

Because photos are obtained from the air with a panoramic view, they can display the entire road network (Figure 2.5 and Figure 2.6). Such a display can provide researchers with a better understanding of how the transportation network interacts with the environment around it. The aerial/satellite photography method can collect inventory data efficiently, and there is no traffic exposure so collection personnel do not need to face dangerous traffic, and the collection process will not distract motorists on the road. However, this method requires crews with professional skills, and the latter data processing step could be quite complicated. In addition, the quality of the collected data is greatly affected by the weather conditions during the collection period.

Figure 2.5 Aerial Photography No.1

Figure 2.6 Aerial Photography No.2

2.5 LiDAR

LiDAR, or 3D laser scanning, is a remote sensing technology that uses laser light to densely sample the surface of the earth. Three types of LiDAR can be used to collect road inventory data, namely, terrestrial LiDAR, mobile LiDAR, and airborne LiDAR. Recent dramatic advances in LiDAR technology have made it quite competitive in science and engineering applications. A detailed description of LiDAR will be presented in Section 3.

3. LIDAR

3.1 What Is LiDAR

LiDAR is a remote sensing technology that collects geometric and geographic information from targets on the earth's surface in the form of point clouds (Figure 3.1). A LiDAR system principally consists of a laser scanner, a specialized GPS receiver, and an IMU system. It uses a principle similar to radar, a better-known technology. The main difference is that, instead of using radio waves or microwaves, LiDAR sends out intense, focused beams of light to measure the distances to the objects. Depending on the wavelength laser used, LiDAR can map a wide range of objects, such as rocks, vegetation, chemical compounds, clouds, and even single molecules. Recent advancements in the LiDAR mapping technique have enabled researchers and mapping professionals to efficiently map large-scale areas with improved accuracy and flexibility.

The history of LiDAR dates back to the early 1960s, shortly after the invention of the laser. LiDAR was first used in meteorology by the National Center for Atmospheric Research (Goyer and Watson, 1963). In the early 1970s, early models of LiDAR were successfully used in the United States, Australia, and Canada. The Ohio Department of Transportation was one of the earliest agencies to employ LiDAR systems in engineering operations (Grejner-Brzezinska et al., 2005). By the end of the 1990s, this technology was occupying a leading position in high-precision spatial data. Compared with other remote sensing technology, LiDAR is more automatic, efficient, and accurate, and can work during both the day and night because laser scanning is relatively independent of sunlight. Since the introduction of LiDAR, this technology has been used for a wide range of applications, including high-resolution topographic mapping (Hill et al., 2000), archaeological sites detecting (Doneus et al., 2013), 3D surface modeling (Zhao et al., 2008), and infrastructure and biomass studies (Chen et al., 2012).

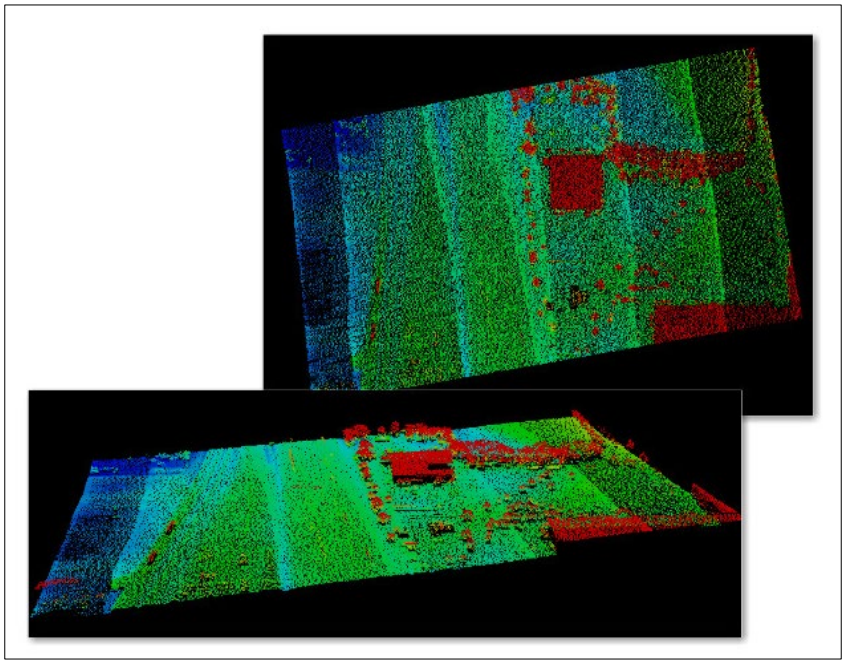

Figure 3.1 LiDAR Point Cloud

3.2 How LiDAR Works

There are two methods to estimate the distance between the LiDAR unit and the target objects: time-of-travel and phase-shift. Time-of-travel scanners transmit pulses and record the time interval between an initial transmission of individual laser pulses and the returning detection of reflected signals to calculate distance values.

$$\text{Distance} = (\text{Speed of Light} \times \text{Time Interval}) / 2 \quad (1)$$

On the other hand, phase-shift scanners calculate distance using the phase-shift principle. A sinusoidally modulated laser pulse is sent out as the laser beam reaches a surface, and then a shift in the signal is detected and registered as a point in the space.

Compared with phase-shift scanners, time-of-travel scanners are rated at much longer ranges, so they are usually used for long-range applications. Phase-shift scanners, however, are limited in range and are generally utilized for indoor or short-range applications despite being faster and more accurate.

The measured distance is then combined with the position and orientation information obtained from integrated GPS and IMU systems to generate the 3D (i.e., latitude, longitude, and altitude, which are also known as the x, y, z coordinates) information about the targeted objects. The x, y, z coordinates of the objects are computed based on:

- the distance between the object and the scanning LiDAR sensor
- the angle at which the laser pulse was "fired"
- the absolute location of the sensor

3.3 LiDAR Classification

Generally speaking, there are three types of LiDAR systems: (1) airborne laser scanning (ALS), (2) mobile laser scanning (MLS), and (3) terrestrial laser scanning (TLS). Each system varies in application, data collection time, cost, and accuracy.

3.3.1 Airborne Laser Scanning (ALS)

ALS is an aerial mapping technology that uses reflected laser returns from the earth's surface with on-board GPS and IMU sensors to generate precise 3D information about terrestrial objects.

Airborne LiDAR is the most commonly available LiDAR, and most airborne LiDAR systems can cover more than 19.3 square miles (50 square kilometers) per hour while the collected data still meet the requirements for high-accuracy data.

As shown in Figure 3.2, airborne systems are capable of scanning perpendicularly to the airplane's flight direction to capture segments of the earth's surface. The laser ranging device sends out millions of pulses to determine the distance between the aircraft and the targets. The GPS provides the location of the instrument holding the LiDAR sensor, and the IMU is used to measure the aircraft's pitch, roll, and heading, which are important for accurate elevation measurements.

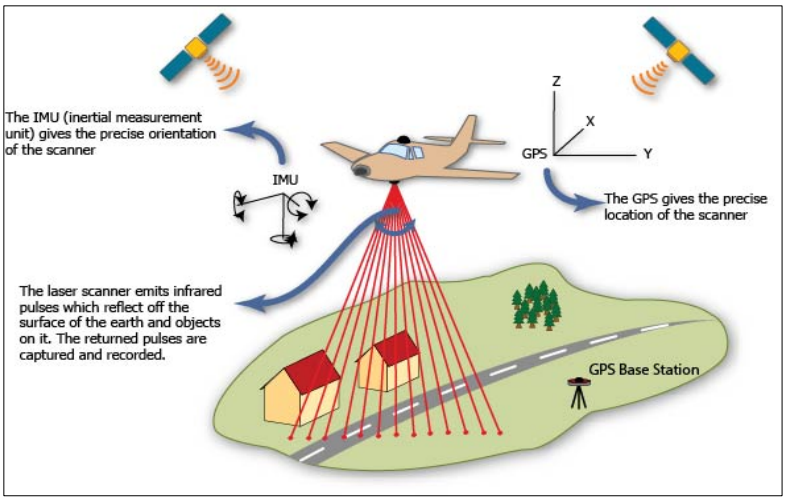

Figure 3.2 Airborne LiDAR System Schematic
(Source: http://gmv.cast.uark.edu/scanning-2/airborne-laser-scanning/)

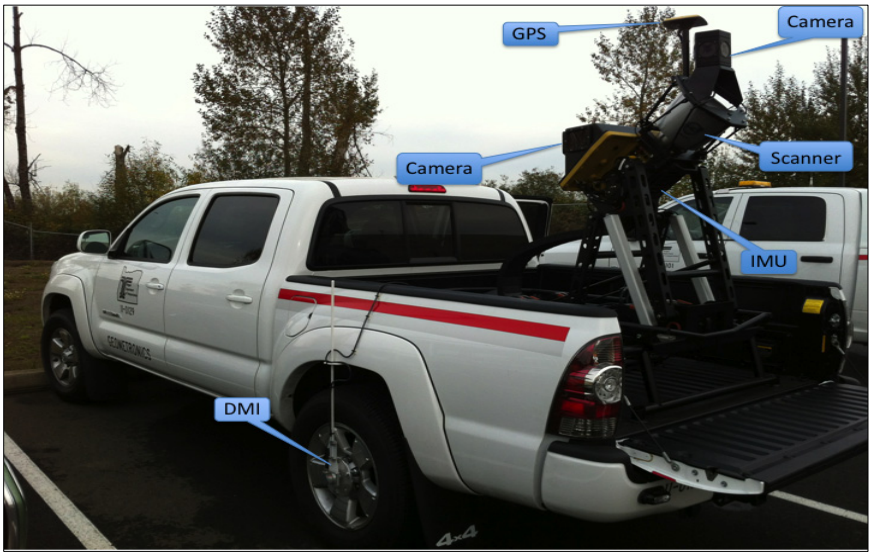

Figure 3.3 Mobile LiDAR System
(Topcon IP-S2 HD system operated by Oregon DOT)

3.3.2 Mobile Laser Scanning (MLS)

MLS is essentially the same as ALS, except that the LiDAR set-up is integrated on a ground-based vehicle, as shown in Figure 3.3. Depending on the range requirement, MLS can use either the time-of-travel or phase-shift method. While driving at highway speeds, current MLS systems are capable of collecting up to one million points per second, including digital imagery and other geospatial data (Williams et al., 2013). This enables MLS systems to provide a dense, geospatial dataset as a 3D virtual world. MLS is efficient in collecting data, and it can minimize traffic disruption as well as safety hazards.

3.3.3 Terrestrial Laser Scanning (TLS)

The fundamentals of laser distance measurement and scanning of TLS are similar to ALS and MLS. TLS is usually operated on a tripod, as shown in Figure 3.4. Because it generally has a relatively smaller range requirement, a TLS system mainly uses phase-shift measurement systems. An ALS system needs only one scanning direction (the other one is accomplished by the moving aircraft), while a terrestrial laser scanner needs a 2D scanning device (Vosselman and Maas, 2010). Because TLS refers to tripod-based measurements, it is stationary and does not need a GPS or INS for direct georeferencing; furthermore, it is able to achieve the highest accuracy among the three types of LiDAR systems.

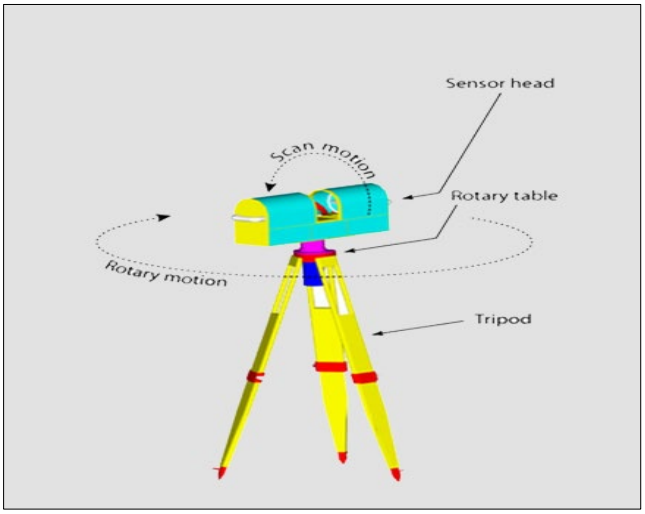

Figure 3.4 Terrestrial LiDAR System
(Source: http://www.bu.edu/tech/support/research/visualization/gallery/lidar/)

3.4 Comparison of LiDAR

The advantages and disadvantages of the three types of LiDAR are summarized in Table 3.1.

Table 3.1 Advantages and Disadvantages of Different Types of LiDAR

	Airborne LiDAR	**Mobile LiDAR**	**Terrestrial LiDAR**
Advantages	High degree of automation Safe operation Less affected by atmospheric conditions Efficient Direct view of pavement and building tops Faster coverage Larger footprint Point density is more uniform High post-processing efficiency	Safe Good view of pavement Direct view of vertical features Higher density Cost-effective	Higher flexibility Higher resolution Higher accuracy Easy to use Highest level of detail
Disadvantages	Poor view of vertical features Lower point density More horizontal positioning uncertainty Could be obstructed by high trees	Cannot capture building tops Cannot detect lower level objects blocked by road surface Slower coverage Small footprint Could be blocked by adjacent large vehicles	Inefficient Lowest cost efficiency Limited to project size

3.5 Airborne LiDAR

3.5.1 Background and History

As early as the beginning of the 1970s, airborne LiDAR systems could reach the precision of less than 3.28 feet (one meter) when measuring distances between aircraft and the earth's surface. However, they were not widely used at that time due to their limited accuracy and measurement range. With the introduction of differential GPS at the end of the 1980s, the position of the scanners could be determined in sub-decimeter range. After that, airborne LiDAR developed very rapidly and became widely used (Vosselman and Maas, 2010).

Many studies and applications have been conducted since the introduction of airborne LiDAR. Baltsavis (1999) provided us with a comprehensive overview of existing systems, vendors, and resources of airborne laser scanning through extensive research. Vosselman and Maas (2010) introduced the principles of airborne and terrestrial laser scanning technology as well as the applications of 3D point clouds collected by laser scanners. This technology is being used for a wide range of applications, including high-resolution topographic mapping and 3D surface modeling as well as infrastructure and biomass studies. Airborne LiDAR data were successfully used by Bernardini et al. (2013) in the mapping of Karstic areas (northeastern Italy), which demonstrates the value of airborne LiDAR technology in landscape archaeology. Swetnam and Falk (2014) used airborne LiDAR to identify individual trees across

large forested landscapes. Doneus et al. (2013) demonstrated the potential of this novel technique to map submerged archaeological structures over large areas in high detail in 3D, providing unique means for underwater heritage management.

3.5.2 Components

The basic components of the airborne laser scanners include the following five parts:

- Flight management system
- Airborne platform
- Laser scanner
- Position and orientation system
- Control and data recording unit (computer)

3.5.3 Flight Management System

The flight management system serves as a means for mission planning and various stages of processing. For example, the pilot can display the preplanned lines through this system, which will give support in completing the mission (Vosselman and Maas, 2010).

3.5.4 Airborne Platform

An airborne platform is a platform for mounting all the data collection hardware. Airplanes and helicopters are the most commonly used platforms for acquiring LiDAR data over broad areas. Helicopters are typically used in the following applications: (1) small width, elongated areas (e.g., power lines, corridor mapping, and topographic and bathymetric mapping along coastlines), (2) small areas (e.g., airports, open pit mines), (3) conditions at very low altitudes (for higher accuracy and denser point measurements) or where low flying speeds are needed (flood mapping), (4) conditions when high maneuverability and many high-curvature turns (e.g., following roads in 3D city modeling) are required, and (5) difficult terrain with abrupt height discontinuities (mountains) (Baltsaias, 1999).

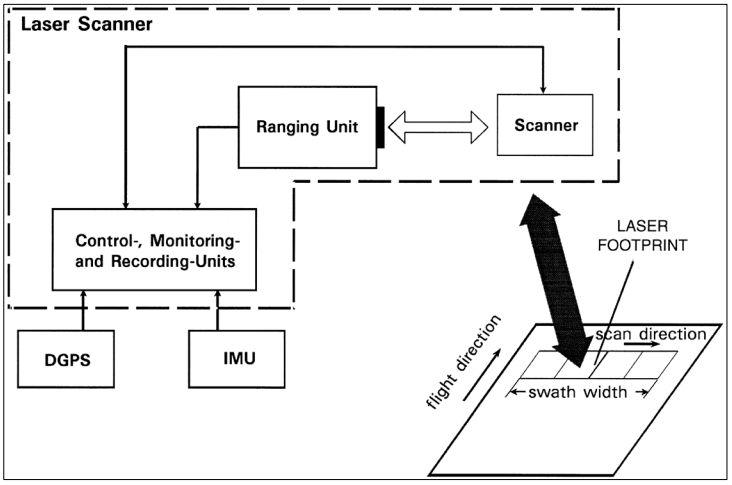

Figure 3.5 Laser Scanner Schematic Unit
(Wehr and Lohr, 1999)

3.5.5 Laser Scanner

The airplane uses a laser beam to scan the earth from side to side as the plane flies. As shown in Figure 3.5, a typical laser scanner can be subdivided into the following key units: laser ranging unit, opto-mechanical scanner, and control and processing unit (Wehr and Lohr, 1999). A medium-sized digital camera that provides image data often works together with laser scanners, because it is difficult to recognize objects using only the range data provided by laser scanners (Vosselman and Maas, 2010). Powerfully pulsed lasers are needed for the measurement of the range because of the relatively large distance between the aircraft and the objectives.

3.5.6 Position and Orientation System

The laser scanner measures only the line-of-site vector from the laser scanner aperture to a point on the earth's surface (Wehr and Lohr, 1999). In order to obtain the 3D position of the target point, the laser scanner system should be supported by a position and orientation system. GPS and IMU are usually used together as the position and orientation system. The GPS antenna is always installed on top of the aircraft to provide an undisturbed view for the GPS satellites, and the IMU is either fixed directly on the laser scanner or close to it (Vosselman and Maas, 2010).

3.5.7 Control and Data Recording Unit

A computer equipped with a display and an operator should be included to provide the control and processing functions for the overall system. The onboard computer also records and stores all of the important information that the LiDAR collects as it scans the earth's surface. By technically using this unit, the operator can set up mission parameters and monitor the performance of the system (Vosselman and Maas, 2010).

Airborne LiDAR systems are always composed with a GPS ground station, which serves as a reference station for achieving decimeter accuracy. During the data collecting process, two GPS ground stations are usually operated, one as the base station and the other as a backup. In recent years, several countries have installed permanent GPS ground stations; thus, normally, there is no need to operate their own GPS stations.

3.6 Applications of ALS in Transportation

3.6.1 Traffic Flow Estimation

Grejner-Brzezinska et al. (2005) conducted a project using airborne LiDAR data for traffic flow estimates. The study presented theoretical and practical studies on the feasibility of using LiDAR data and airborne imagery collected over the transportation corridors for the estimation of traffic flow parameters. They proved that high-point density airborne LiDAR can effectively support traffic monitoring and management by delivering a variety of traffic flow data.

3.6.2 Highway Corridor Mapping

Uddin and Al-Truk (2001) presented the application of airborne LiDAR technologies for the cost-effective management of highway corridors, airports, and related transportation infrastructure assets. They produced digital terrain models, generated digital mapping databases, and linked various data sources through user-friendly GIS software. In their study, they introduced a real case study of the Raleigh bypass highway alignment project. The study also carried out a high resolution and accurate digital terrain mapping for Oxford and surrounding areas in northern Mississippi by applying the airborne LiDAR

technology to illustrate the data accuracy, efficiency, and cost-effectiveness of the airborne laser technology.

3.6.3 Integrated Uncertainties of Traffic Island Modeling

Affecting traffic behavior safety, air pollution, and transport decision support, traffic islands play a major role in transport studies. Zhou and Stein (2013) used airborne laser scanning data to develop a random set approach to determine the locations of traffic islands. The study showed that point spacing makes the largest contribution to the positional accuracy of a traffic island.

3.6.4 Collecting and Recording Highway Inventory

Zhou et al. (2013) compared various technologies of collecting highway inventory data to determine the most cost-effective method. These technologies include field inventory, photo/video logs, integrated GPS/GIS mapping systems, aerial photography, satellite imagery, virtual photo tourism, terrestrial laser scanners, and mobile mapping systems (i.e., vehicle-based LiDAR, and airborne LiDAR). They concluded that mobile LiDAR can quickly collect all required feature data, but it requires an extensive data reduction effort and has the ability to collect data valuable for multiple DOT programs.

3.6.5 Expanding Highway Projects

The application of airborne laser technology in Uddin's paper demonstrated that ALS is an efficient and economical way of collecting data (Uddin, 2008). They compared the elevation data accuracy, efficiency, and cost-effectiveness with the traditional aerial photogrammetry and ground-based total station survey methods. This research recommended that traditional methods should be combined with low-altitude airborne laser technology to save money and time for highway projects.

4. FIELD EXPERIMENT AND DATA COLLECTION

4.1 Methodology

The objective of this project is to evaluate the pros and cons of the airborne LiDAR system in gathering road inventory data. The Remote Sensing Service Laboratory (RSSL) at Utah State University (USU) carried out the data collection campaign.

The USU airborne LiDAR system is mounted in a single engine Cessna TP206 aircraft (Figure 4.1). The system consists of a LiDAR scanner, IMU, and flight navigation unit (Figure 4.2). The LiDAR instrument consists of a Riegl Q560 transceiver and Novatel SPAN LN-200 GPS/IMU positioning and orientations system. Depending on the flight height, the LiDAR scanner is able to collect data at a pulse rate of 250,000 shots/seconds. Together with the LiDAR system, the USU airborne system is also equipped with multispectral and thermal infrared cameras, which can be used for aerial photos. The camera system is composed of four ImperX 4820 Monochrome cameras with 4,872 x 3,248 pixels per camera. They are also equipped with interface filters in the blue, green, red, and near-infrared (NIR) centered at 0.472 μm, 0.562 μm, 0.655 μm, and 0.80 μm, respectively.

Figure 4.1 The USU Cessna TP206 Research Aircraft

Figure 4.2 The Onboard Integrated Remote Sensing System

4.2 Data Collection

This part of the study summarizes the field experiments conducted by the RSSL at USU. Prior to data acquisition, the flight lines were planned and stored in the onboard GPS system to be followed during the actual flight. The flight campaign was conducted on June 4, 2015, and can be divided into two separate parts. The first was from 11:20 a.m. to 12:45 p.m. and covered three road sections: Interstate 84 (I-84), Interstate 15 (I-15) North, and I-15 South. The second part, from 3:20 p.m. to 4:20 p.m., mapped section US-191. The weather conditions were a partially cloudy sky and a clear sky during the first and second parts of the flight, respectively.

Each section of the roads of interest was divided into multiple subsections, each covered by a single flight line. The data acquisition includes LiDAR and colored high resolution images. The study covered these four road sections in Utah: one on I-84, two on I-15, and one on US-191 (Figures 4.3-4.4). The exact location of these sites can be described by the distance between two mileposts (MP) as follows:

- I-84 from Mountain Green to Morgan County/Summit County (MP 97 to 113)
- I-15 North from Lehi to Salt Lake City (MP 284 to 307)
- I-15 South from Santaquin to Springville (MP 241 to 260)
- US-191 from MP 84 to 112 (MP 84 to 112)

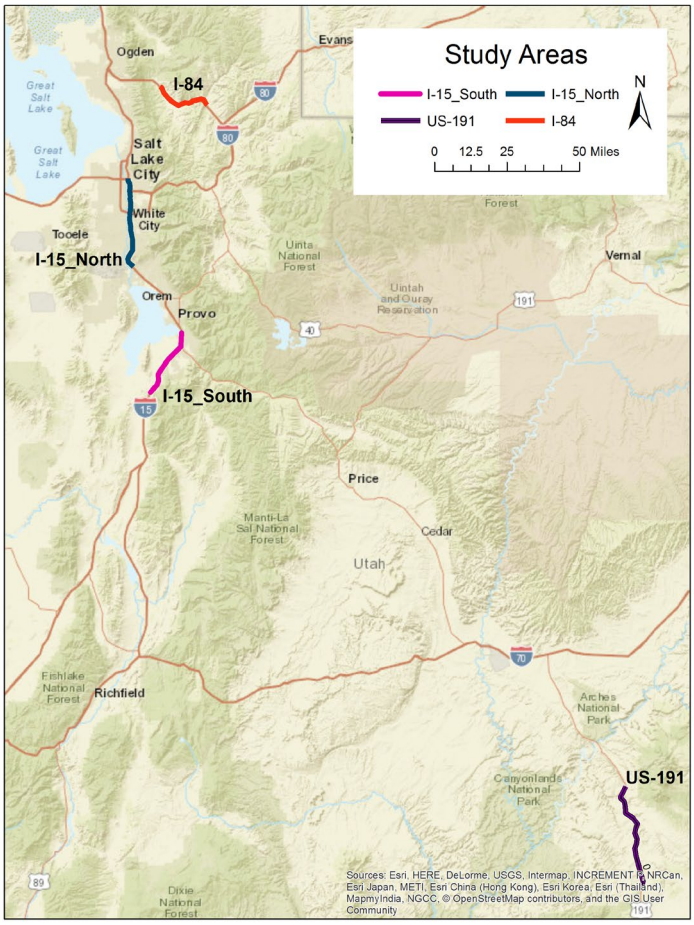

Figure 4.3 Layout of the Mapping Areas

Site 1: I-84 from Mountain Green to Morgan County/Summit Country

Site 2: I-15 North from Lehi to Salt Lake City

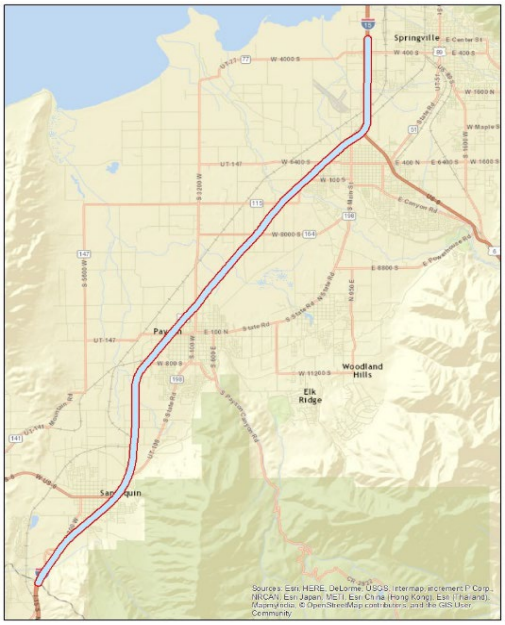

Site 3: I-15 South from Santaquin to Springville

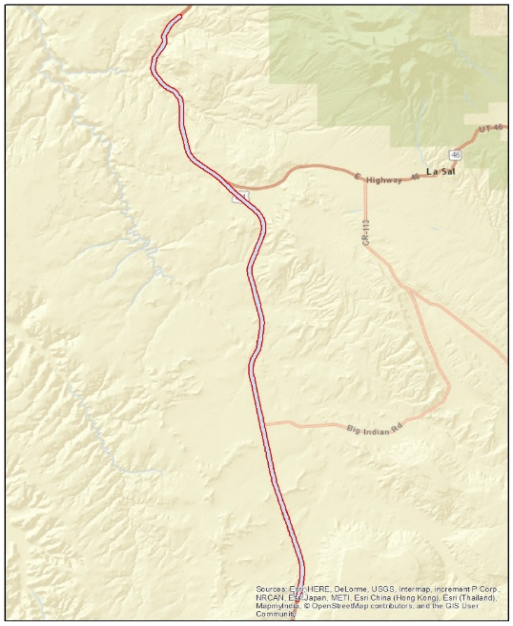

Site 4: US-191 from MP 84 to 112

Figure 4.4 Layout of the Surveyed Road Sections

The data were acquired at an average flight height of approximately 1,640 feet (500 meters) above ground level (AGL) or lower. The LiDAR scan rate was about 125 Hz, the pulse rate was 200,000 shots/second, and average flight speed was about 112 mph (180 km/h). In these settings, the point density can be up to 0.6 points/ft^2. In total, four bands of multispectral data were acquired by the cameras, red, green, blue, and NIR. The lists of raw LiDAR data for I-84, I-15 North, I-15 South, and US-191 are given in the following two tables. Because there are a large number of imagery data files, we decided not to list them here.

Table 4.1 Raw LiDAR Data Files for I-84, I-15 North, and I-15 South

No	File name	No	File name	No	File name
1	150604_172316.las	**12**	150604_181243.las	**23**	150604_184006.las
2	150604_172716.las	**13**	150604_181603.las	**24**	150604_184249.las
3	150604_173001.las	**14**	150604_181830.las	**25**	150604_185420.las
4	150604_173255.las	**15**	150604_182123.las	**26**	150604_185716.las
5	150604_173438.las	**16**	150604_182332.las	**27**	150604_190007.las
6	150604_173631.las	**17**	150604_182545.las	**28**	150604_190536.las
7	150604_174345.las	**18**	150604_182708.las	**29**	150604_190838.las
8	150604_174737.las	**19**	150604_183024.las	**30**	150604_191047.las
9	150604_174928.las	**20**	150604_183259.las	**31**	150604_191329.las
10	150604_175150.las	**21**	150604_183538.las		
11	150604_181046.las	**22**	150604_183745.las		

Table 4.2 Raw LiDAR Data Files for US-191

No	File name	No	File name
1	150604_220311.las	**12**	150604_213710.las
2	150604_220453.las	**13**	150604_213816.las
3	150604_220648.las	**14**	150604_214020.las
4	150604_221114.las	**15**	150604_214252.las
5	150604_221513.las	**16**	150604_214525.las
6	150604_212453.las	**17**	150604_214900.las
7	150604_212659.las	**18**	150604_215123.las
8	150604_212904.las	**19**	150604_215407.las
9	150604_213115.las	**20**	150604_215759.las
10	150604_213324.las	**21**	150604_220028.las
11	150604_213516.las		

4.3 Data Preprocessing

The raw airborne LiDAR data and imagery data were preliminarily processed and evaluated by the RSSL at USU. They used the Waypoint Inertial Explorer software (www.novatel.com) to process the raw GPS/IMU data and the GPS data, which were obtained from the onboard navigation system and the international global navigation satellite system (GNSS) (https://igscb.jpl.nasa.gov/) service (IGS) base stations, respectively. From these datasets, they could get the position and the altitude of the aircraft. Four IGS base stations were chosen based on their proximity to the four highway segments. The coordinates of the IGS base stations established a geo-position relative to the WGS84 datum during the data collection process and generated the navigation message.

The flight trajectory data were transformed to the WGS84 datum. Figure 4.5 presents the whole flight trajectory for the entire data collection. Figure 4.6 presents the separate flight trajectories for each highway segment.

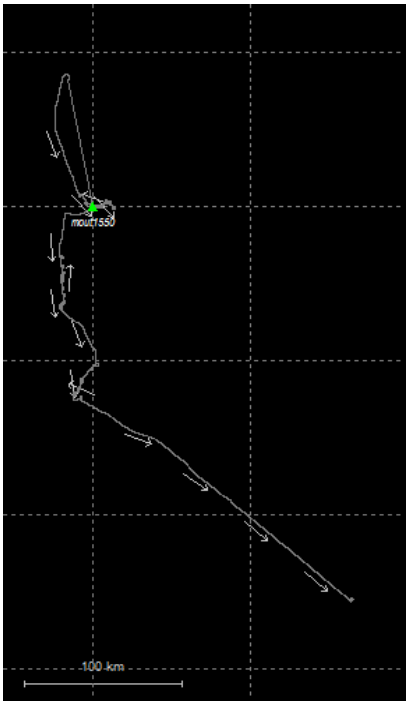

Figure 4.5 The Whole Flight Trajectory for the Entire Data Collection

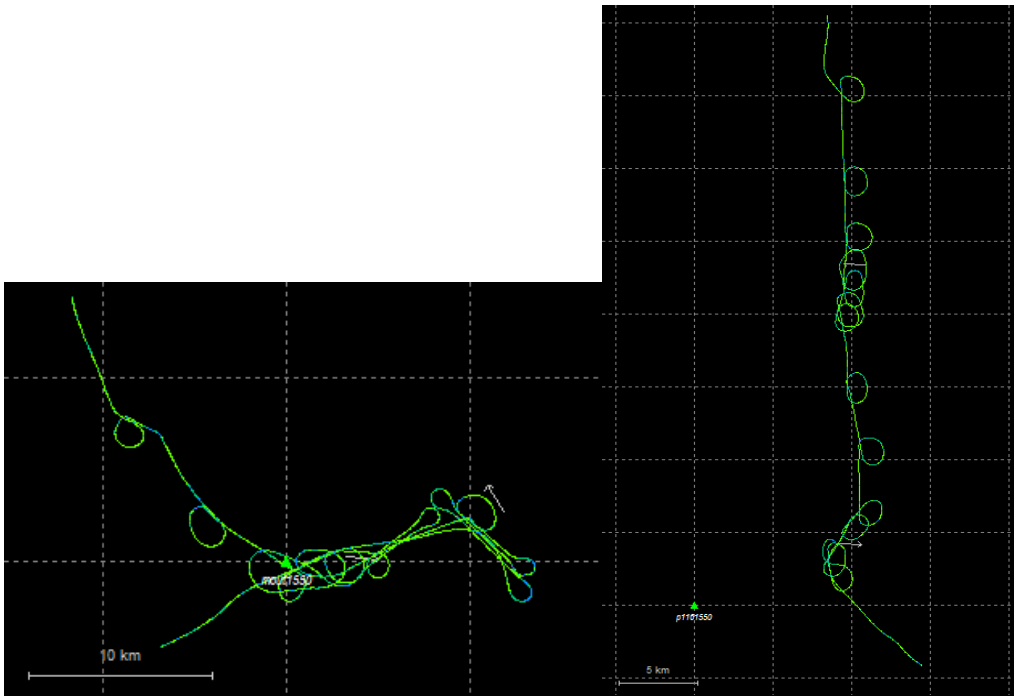

Site 1: I-84 Site 2: I-15 North

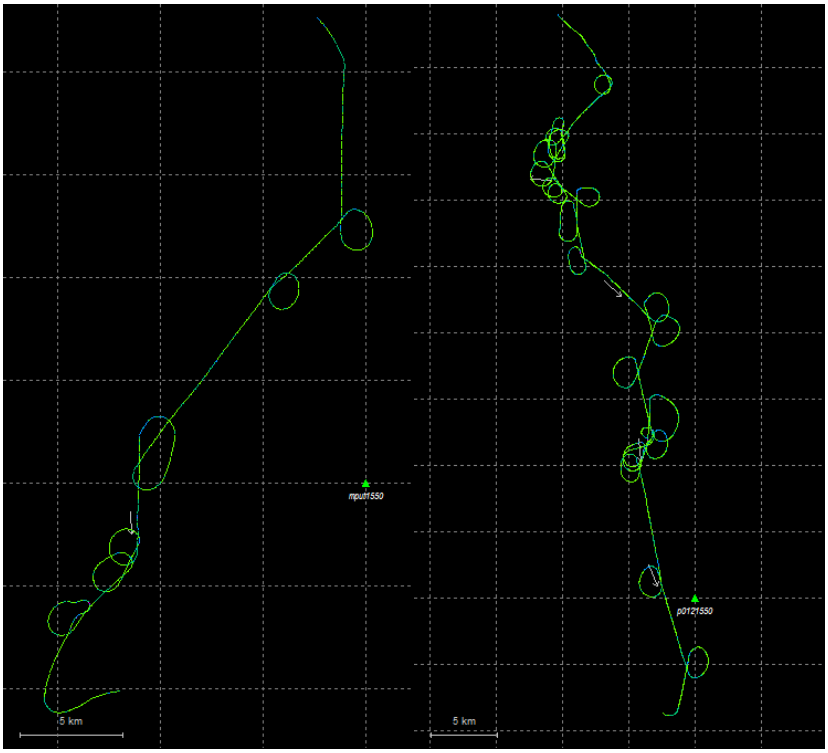

Site 3: I-15 South Site 4: US-191

Figure 4.6 The Separate Flight Trajectories for Four Sections

The aircraft trajectories were also processed in time. The separations of the aircraft trajectories are shown in Figure 4.7, where the east, north, and up directions (x, y, and z coordinates) were presented by red,

green, and blue colors, respectively, and the peak/high separation values respected the direction changes or turns.

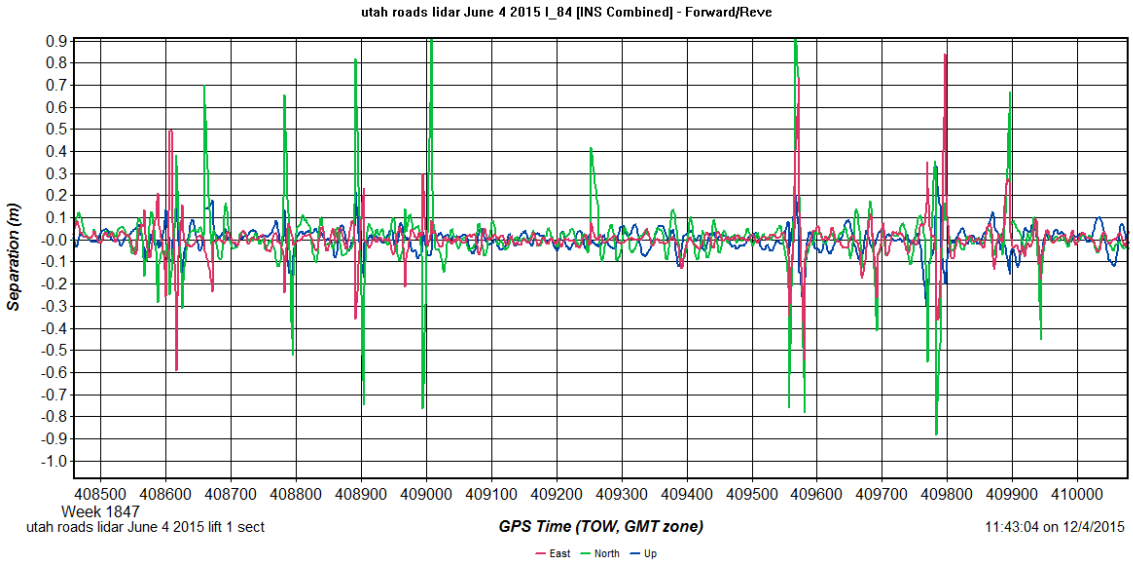

Site 1. I-84

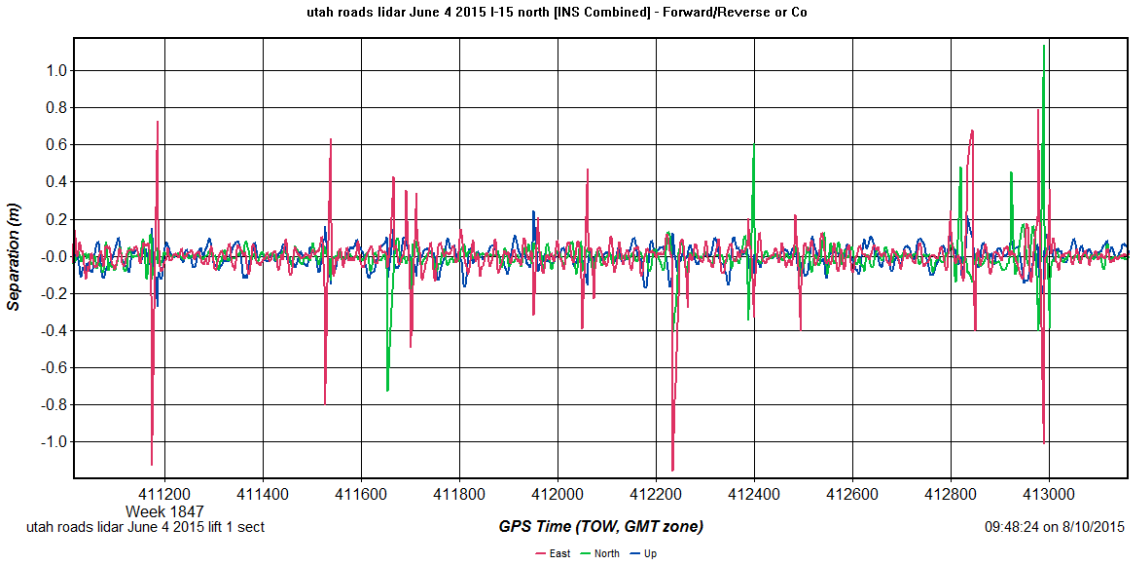

Site 2. I-15 North

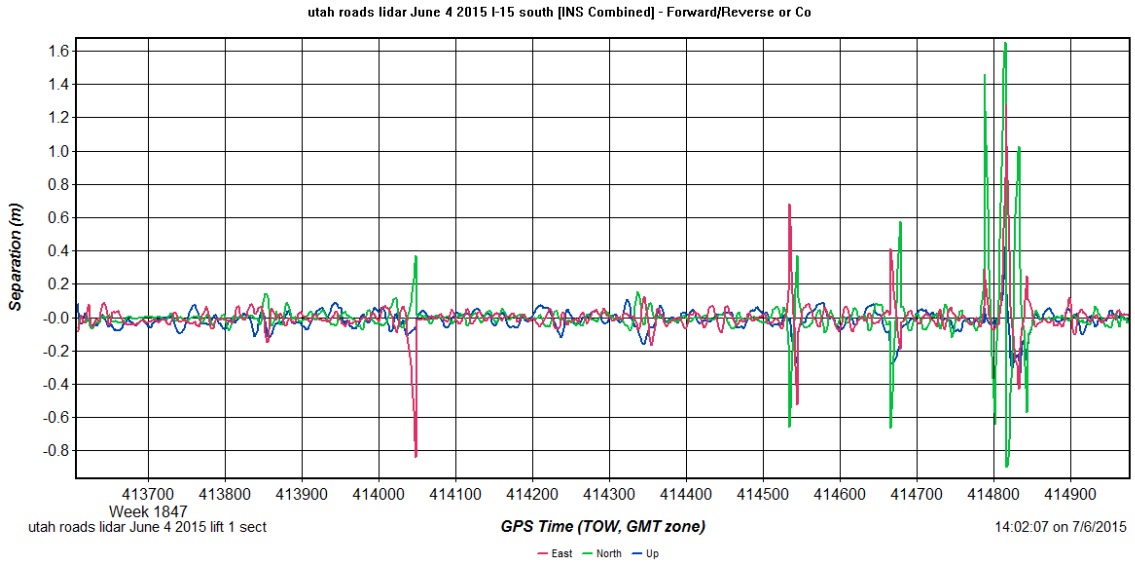

Site 3. I-15 South

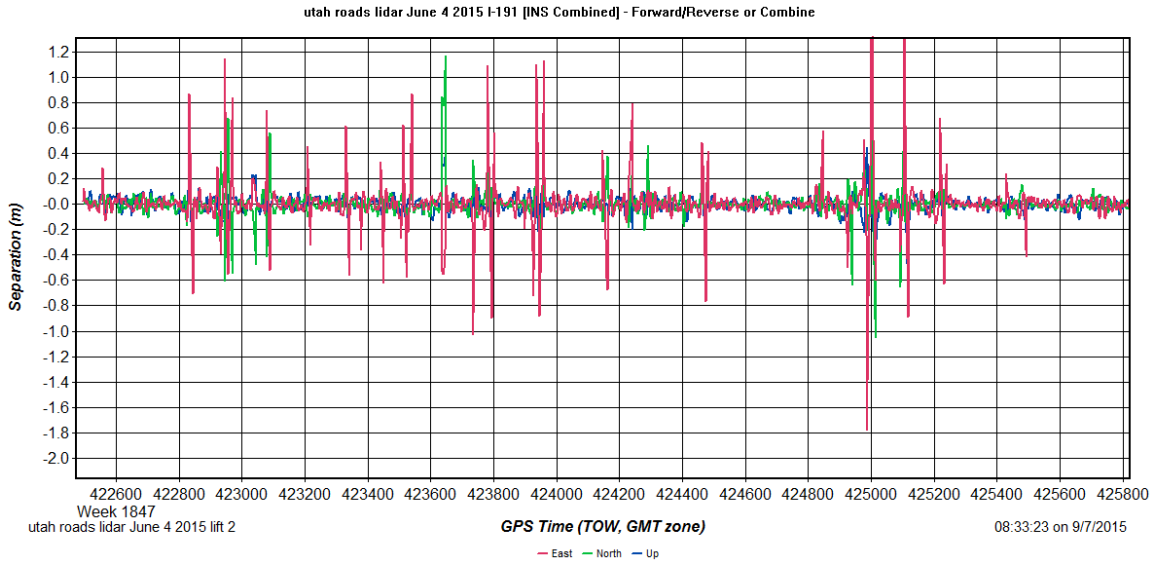

Site 4. US-191

Figure 4.7 Flight Trajectory Separation in Time

The RiAnalyze software was used to analyze the collected LiDAR data and transform the LiDAR full waveform data to point cloud data. Then the RiProcess software was used to add the x, y, z coordinates to the point cloud data. The RiProcess software was also used to perform data calibration and strip (single scan line) adjustment to improve data accuracy. Because each flight line was processed individually, it was possible for the data analyst to ensure quality control (QC) for the overlap between lines.

4.4 Accuracy of LiDAR Data

We used the U.S. Geological Survey (USGS) National Geospatial Program (NGP) standard to evaluate the LiDAR data accuracy. This standard places unprecedented emphasis on LiDAR point cloud data. The basic requirements for LiDAR point cloud data according to the USGS NGP standard are shown in Table 4.3.

Table 4.3 Summary of USGS NGP Guidelines v.13 for LiDAR Data Quality

RMSE	Condition	Source
4.9 in (12.5 cm)	Fundamental vertical accuracy (in the clear)	USGS
3.9 in (10.0 cm)	Within swath overlap regions	USGS
2.8 in (7.0 cm)	Relative accuracy within individual swaths	USGS

Two methods are used to evaluate the accuracy of the LiDAR data. One evaluates the differences between the flight trajectory obtained from the onboard GPS/IMU system and the flight trajectory obtained from the ground-based IGS station. The other one evaluates the elevation differences of different flight strips within their overlapping areas. However, during the data acquisition process, no ground control point information was collected. Hence, we cannot use the flight trajectory solution to estimate data accuracy. But according to Figure 4.7, the average forward/reverse or combined separation is less than 2.0 inches (5 cm), which generally means that fundamental vertical accuracy (in the clear) of 4.9 inches (12.5 cm) can be achieved.

The error within swath overlap regions can be calculated by comparing the differences between flight lines in their overlapping areas. Figures 4.8 through 4.11 show the flight lines for one highway section and use one overlapping area for error evaluation; the evaluation result is provided in a histogram.

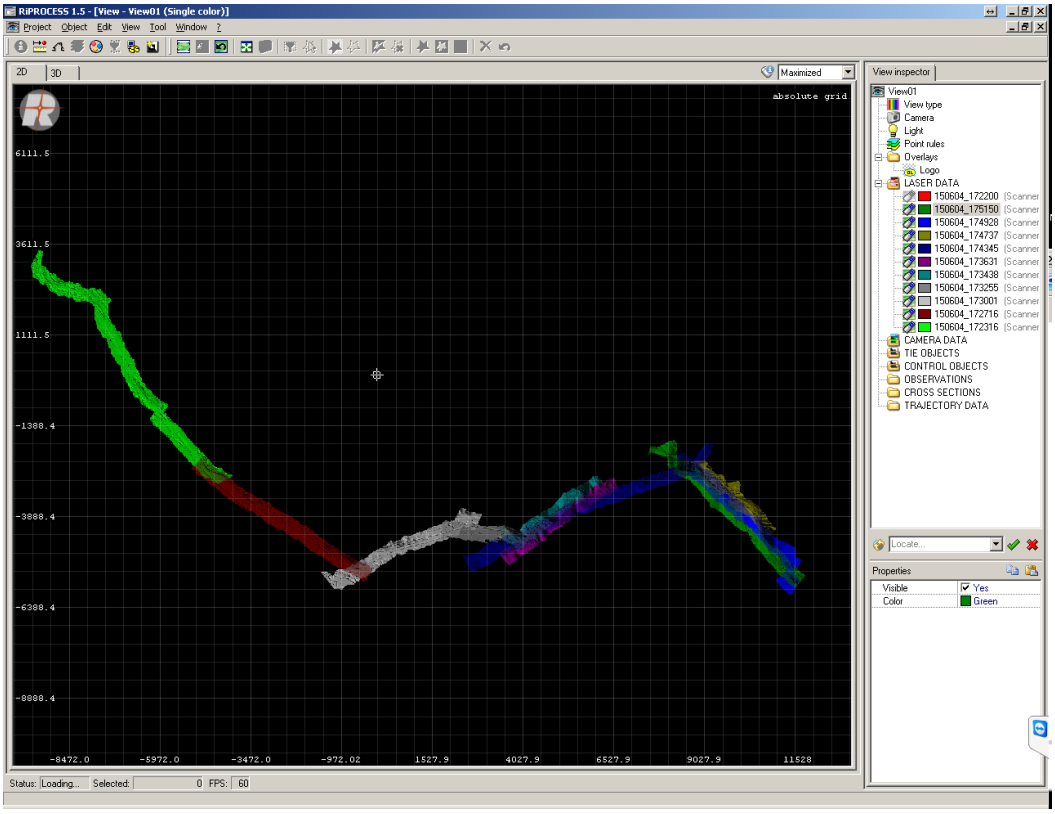

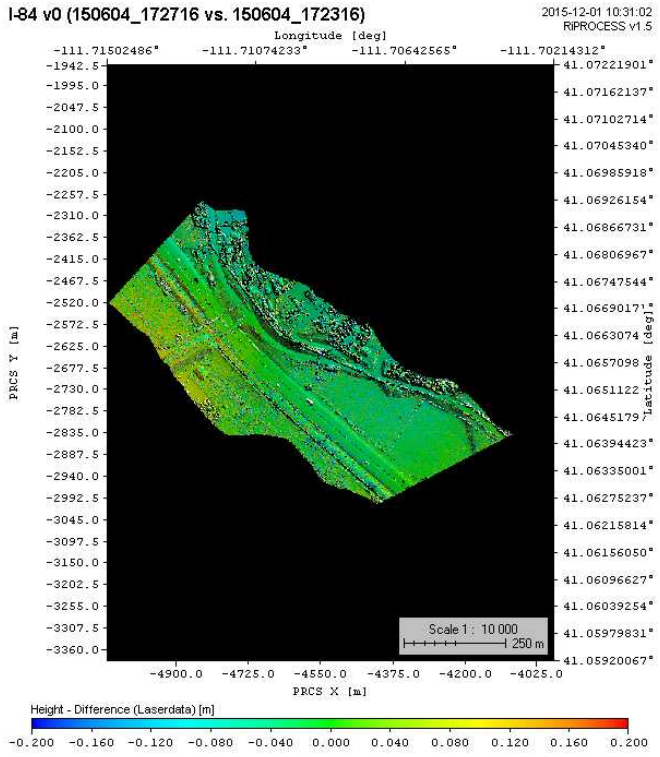

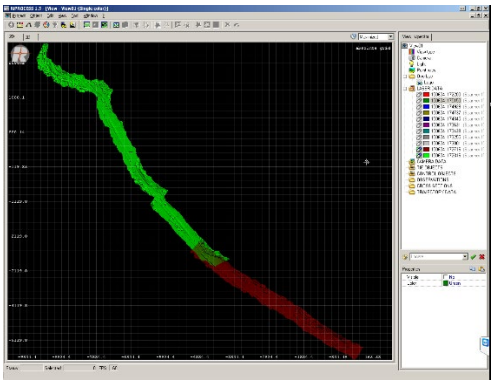

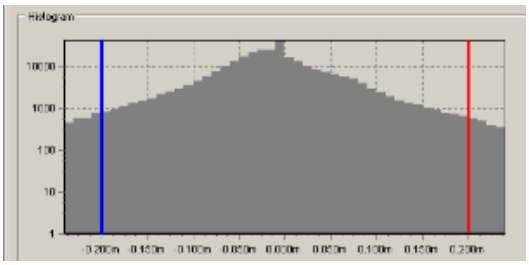

Figure 4.8 Site 1. I-84

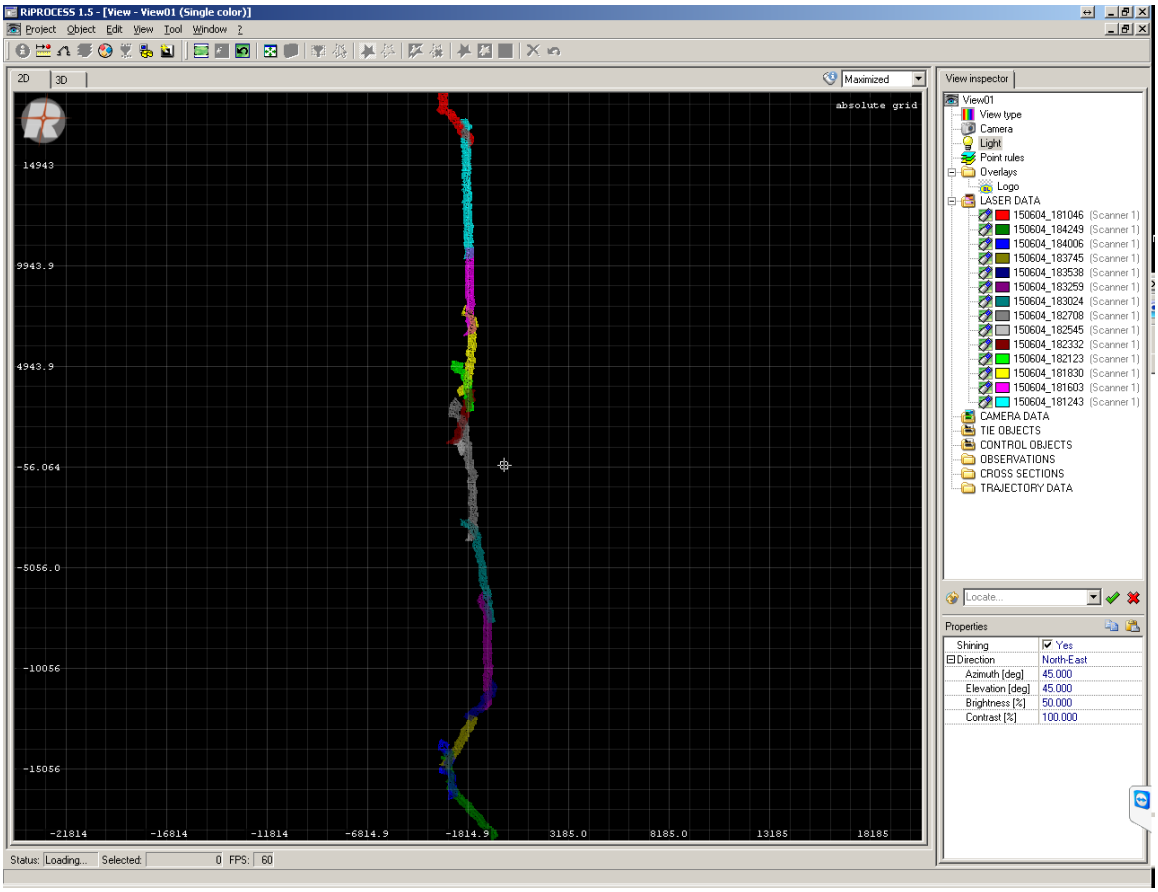

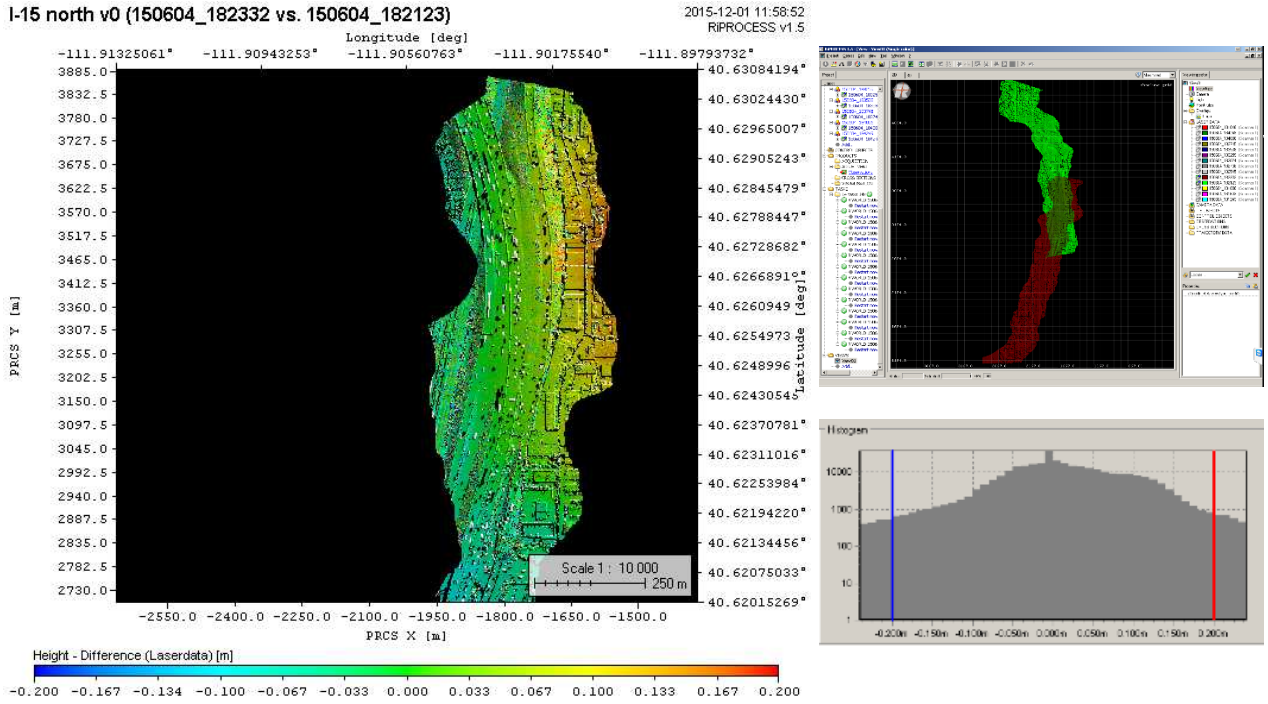

Figure 4.9 Site 2. I-15 North

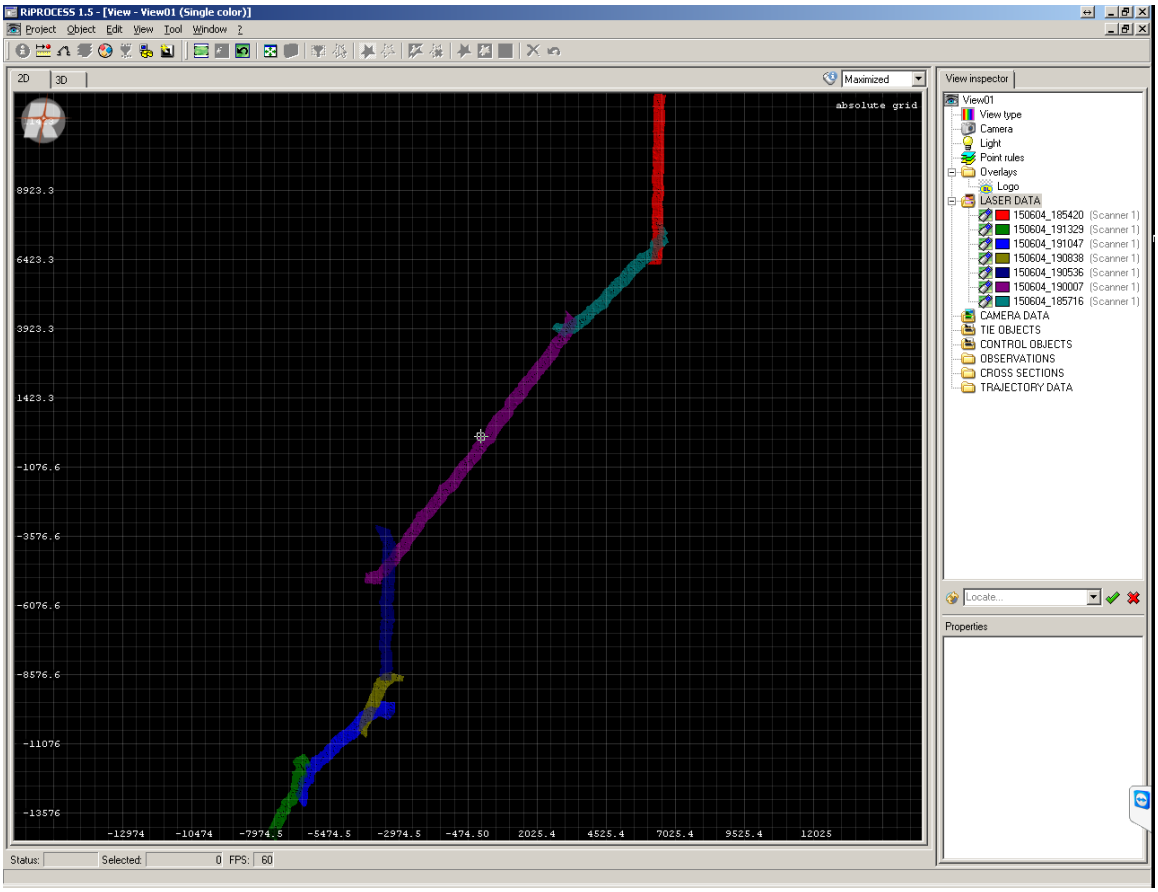

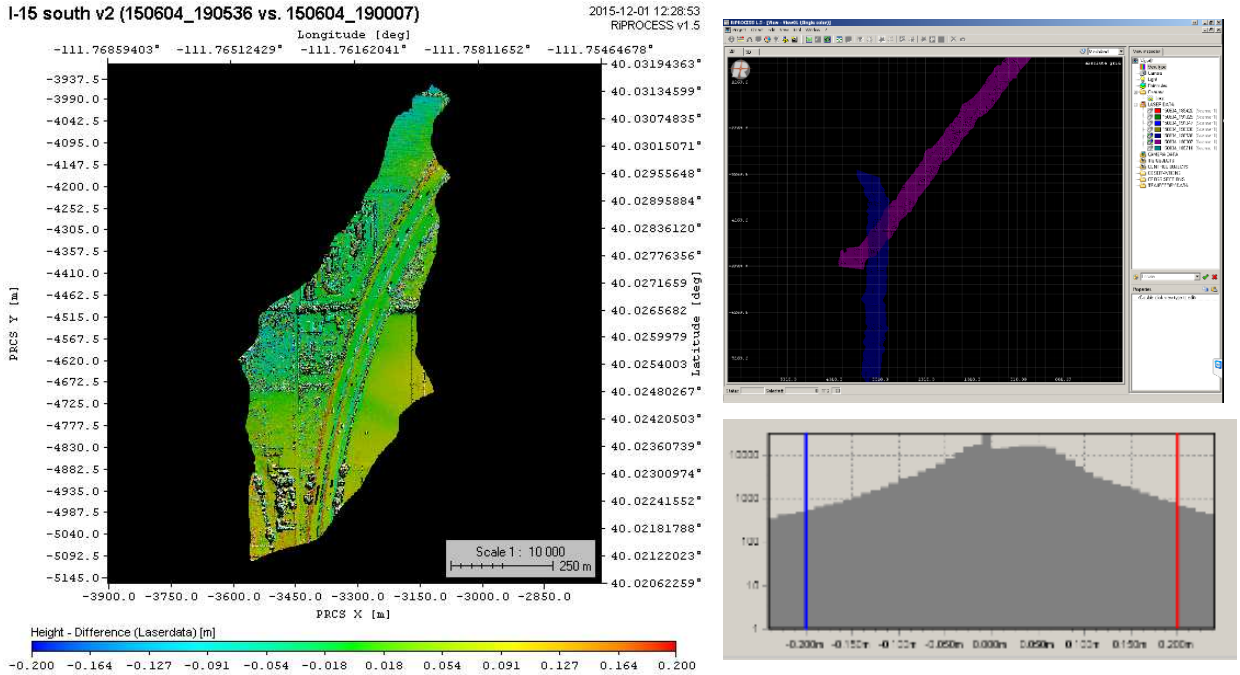

Figure 4.10 Site 3. I-15 South

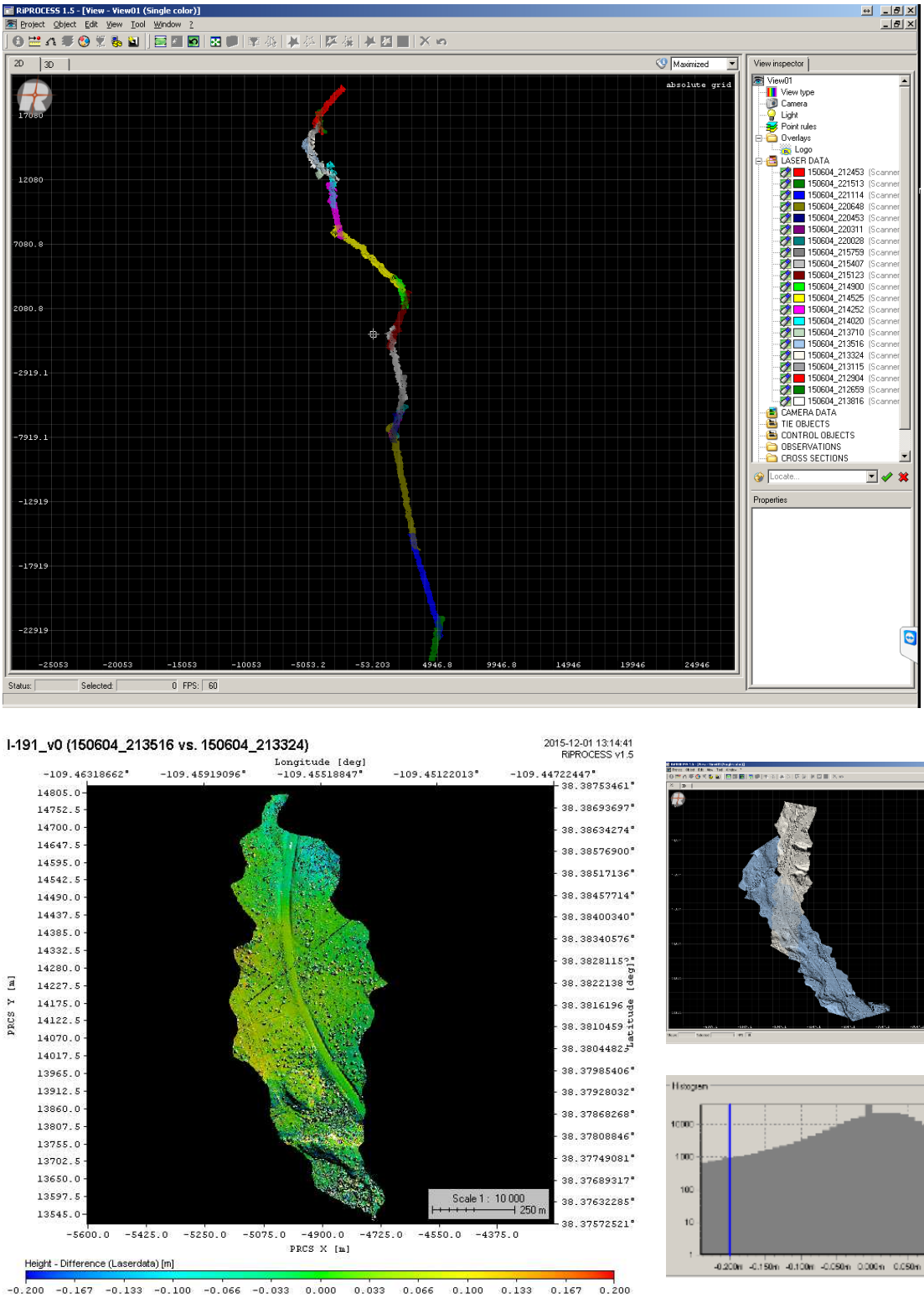

Figure 4.11 Site 4. US-191

The associated RMSE for each of the road sections (i.e., I-84, I-15 North, I-15 South, and US-191) was calculated to be 3.3 in., 3.0 in., 3.2 in, 2.4 in. (8.3, 7.6, 8.2, and 6.2 cm), respectively. The average RMSE was 3.0 in. (7.6 cm), which is smaller than 3.9 in. (10 cm) as required by the USGS standard. Thus, the accuracy standard within the swath overlap regions was achieved.

Generally speaking, the relative accuracy within individual swaths will not be greater than the overlap regions' accuracy. Hence, the relative accuracy within the swath can be estimated to be less than the RMSE of 3.0 in. (7.6 cm) on average.

A summary of the LiDAR data accuracy assessment is shown in Table 4.4.

Table 4.4 Summary of LiDAR Data Accuracy Assessment

RMSE Requirement	Condition	Estimated RMSE Achieved
2.8 in. (7.0 cm)	Relative accuracy within individual swaths	Less than 3.0 in. (7.6 cm) estimated
3.9 in. (10.0 cm)	Within swath overlap regions	3.0 in. (7.6 cm) average measured
4.9 in. (12.5 cm)	Fundamental vertical accuracy (in the clear)	Not assessed but was likely achieved

5. AIRBORNE LIDAR DATA PROCESSING USING ARCGIS

5.1 Introduction

After preprocessing, LiDAR data can be used to extract information, such as the height and location of various highway assets. Several kinds of software can process LiDAR data, including FugroViewer and ArcGIS. FugroViewer is a 3D geodata viewer; it can read LiDAR data and provide some basic tools to extract information from the data. ArcGIS is developed by Esri for working with maps and geographic information. Once the data have been acquired as a vector file, a raster file, or a LAS file, they can be viewed and operated in ArcGIS. In this section, we developed an ArcGIS-based algorithm to detect highway assets from the obtained LiDAR data.

Highway assets include traffic signs, traffic signals, billboards, light poles, guardrails, bridges, culverts, and more. As previously mentioned, LiDAR is a remote sensing technology that collects geometric and geographic information of targets on the earth's surface in the form of point clouds. In LiDAR data, an object can only be identified based on its corresponding points. Thus, if an object has no or very few corresponding points, we cannot properly identify it. The point density of the obtained LAS files is around 0.6 points/ft^2 (6 points/m^2). Small traffic signs, such as speed limit signs and instruction signs (Figures 5.1-5.2), have areas usually less than 10 ft^2 (1 m^2). Moreover, there is an angle (less than 90 degrees) between the laser beams and the signs during scanning. Therefore, there may be only one or two points representing a sign. We can hardly identify an object based on one or two points, thus it is impossible for us to detect those small signs simply by using airborne LiDAR data. However, large traffic signs, especially those with large assemblies, are fairly conspicuous in LiDAR data. Figure 5.3 shows a picture of an overhead traffic sign and Figure 5.4 shows its corresponding LiDAR data. We can observe that, although the sign's face cannot be clearly seen in LiDAR data, the large sign assembly represented by a series of points can be easily identified. Similarly, small traffic signals are not clear in LiDAR data (as shown in Figure 5.5 and Figure 5.6), while traffic signals with large assemblies can be identified in LiDAR data (as shown in Figure 5.7 and Figure 5.8). In addition, light poles usually are vertical structures; they can also be identified in LiDAR data (as shown in Figure 5.9 and Figure 5.10). Billboards usually have large faces and assemblies, making them very conspicuous in LiDAR data (as shown in Figure 5.11 and Figure 5.12). Since airborne LiDAR technology maps target objects from the air, highway structures, including bridges and culverts, can also be seen in airborne LiDAR data. Figure 5.13 and Figure 5.14 show a picture of a bridge and its profile in LiDAR data, respectively. Figure 5.15 and Figure 5.16 show a culvert and its profile in LiDAR data, respectively. Barriers are also very important subsidiary facilities for highways. Different types of barriers exist, such as cable barriers, box beam barriers, and constant slope concrete barriers. In the collected airborne LiDAR data, all kinds of barriers can be easily identified, except for cable barriers with a small surface area. Figure 5.17 shows a section of cable barriers, and Figure 5.18 shows its profile in collected LiDAR data. Cable barriers can hardly be seen in LiDAR data. As shown in Figure 5.19 and Figure 5.20, a segment of W-beam barriers corresponds to a long string of points above ground in LiDAR data.

Figure 5.1 Speed Limit Sign

Figure 5.2 Instruction Sign

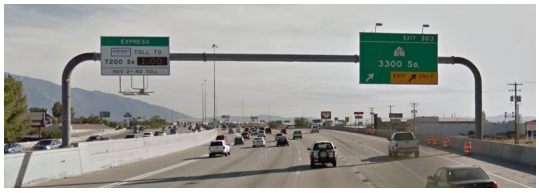

Figure 5.3 Overhead Traffic Sign

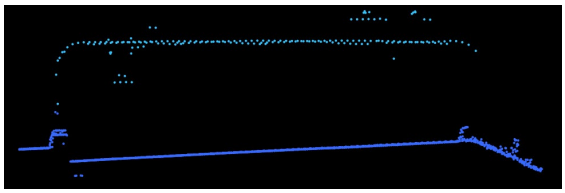

Figure 5.4 Overhead Traffic Sign in LiDAR Data

Figure 5.5 Small Traffic Signal

Figure 5.6 Small Traffic Signal in LiDAR Data

Figure 5.7 Large Traffic Signal

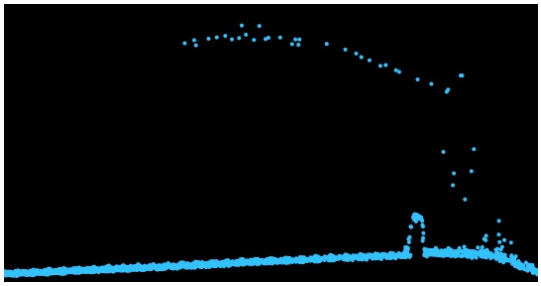

Figure 5.8 Large Traffic Signal in LiDAR Data

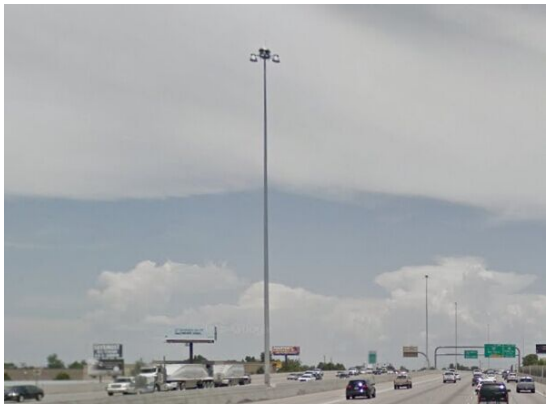

Figure 5.9 Light Pole

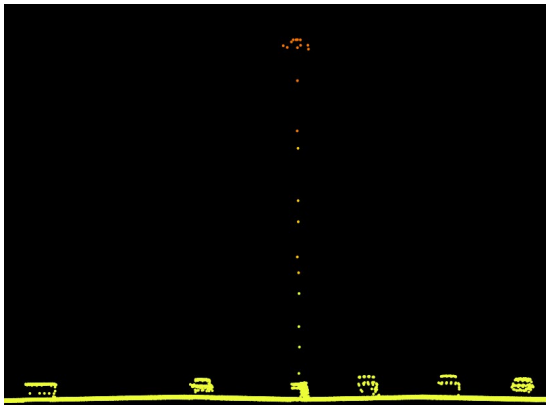

Figure 5.10 Light Pole in LiDAR Data

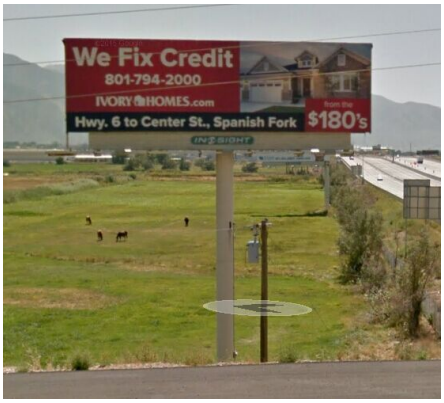

Figure 5.11 Billboard

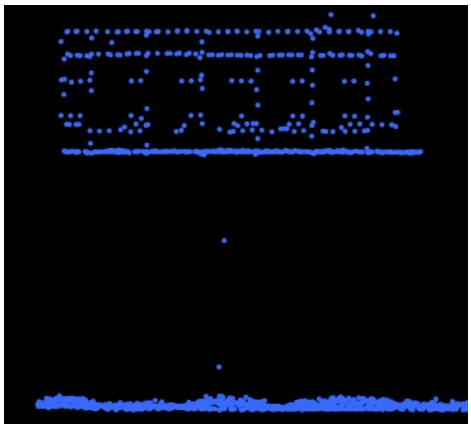

Figure 5.12 Billboard in LiDAR Data

Figure 5.13 Bridge

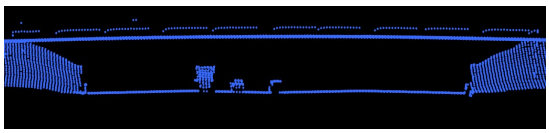

Figure 5.14 Bridge in LiDAR Data

Figure 5.15 Culvert

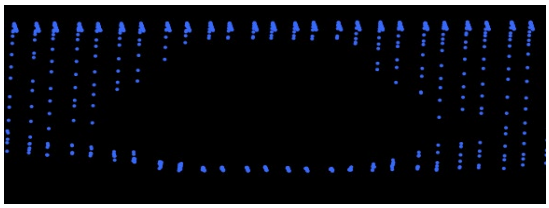

Figure 5.16 Culvert in LiDAR Data

Figure 5.17 A Section of Cable Barrier

Figure 5.18 Cable Barrier in LiDAR Data

Figure 5.19 W-beam Barrier

Figure 5.20 W-beam Barrier in LiDAR Data

For all the above-mentioned road assets that can be identified in airborne LiDAR data, their specific location information and structure characteristics can be manually measured and recorded in the LiDAR data. However, manually identifying all the road features requires a great deal of time and effort; meanwhile, it may lead to some omission due to human error. Therefore, we developed an ArcGIS-based algorithm to extract certain types of road features from airborne LiDAR data. Based on the algorithm, we first used ArcGIS to automatically find all specific road assets, and then measured and recorded their location and structural information.

5.2 ArcGIS-based Feature Extraction Algorithm

The algorithm we developed for extracting road assets is based on the elevation difference between the assets and the bare ground. The algorithm consists of the following steps:

1) Load LAS files (airborne LiDAR data) to ArcGIS. Divide the LAS data into small square cells of a certain size. For each small cell, calculate the elevation difference between the highest point and the lowest point within that cell. This procedure can be done using the LAS Point Statistics as Raster tool in ArcGIS. The result will be raster data, within which each cell has a particular value: the elevation difference.

2) Evaluate the range of elevation difference between a certain type of road asset and the bare ground. Delete all the cells that are out of the range from the obtained raster data.

3) Determine a road boundary and clip the raster data from step (2) according to the boundary to remove the cells beyond the road.
4) Further convert the raster data from step (3) into feature data.

Figure 5.21 shows the flowchart of this algorithm.

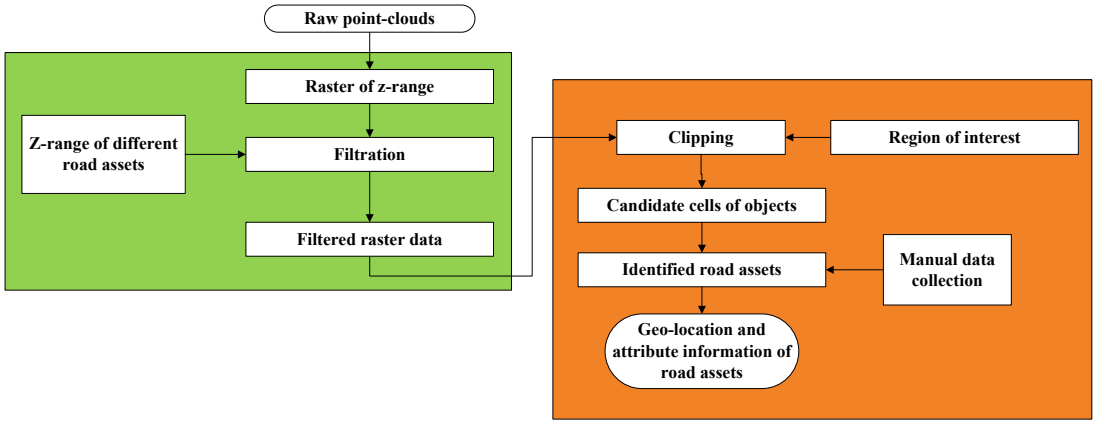

Figure 5.21 Flowchart of ArcGIS-based Algorithm

In this report, we used a large traffic sign as an example to show the effectiveness of the proposed algorithm. Figure 5.22 shows a section of the original LAS data in ArcGIS. We can hardly identify anything from the raw data. We then transformed the LAS data into raster data using the LAS Point Statistics as Raster tool (step 1). The obtained raster data are shown in Figure 5.23. Then we can use the raster-based tools in ArcGIS to deal with the raster data. In this research, we chose 1 as the cell size of the raster data (i.e., each cell of the raster data has an area of 1 m^2). It can be seen from Figure 5.23 that most cells have values near zero. As previously mentioned, the value of a cell represents the elevation difference between the highest point and the lowest point within that cell; thus, a cell with a value near zero means all the LAS points within that cell have a similar elevation. For the cells that contain points representing a large traffic sign, the values should be near the height of the traffic sign. The height of traffic signs can be directly measured from LAS data, or can be estimated based on highway design specifications. If we remove all the cells whose values fall into a certain range (e.g., smaller than the height value of the traffic sign), the remaining cells should be the candidate cells that may contain points representing the traffic sign (Figure 5.24). We then clipped out all the cells that were within the range of the road surface, as traffic signs should be in the range of the road surface (Figure 5.25). From Figure 5.25, we can easily detect the traffic sign and then record the location and structural information of the traffic sign.

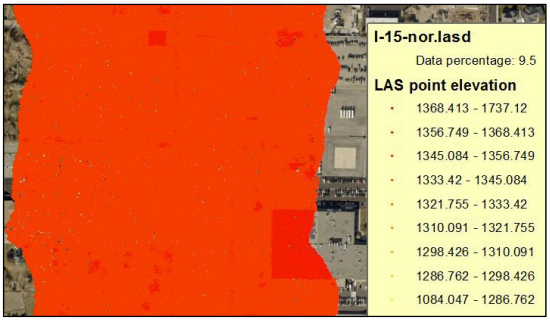

Figure 5.22 LAS Data

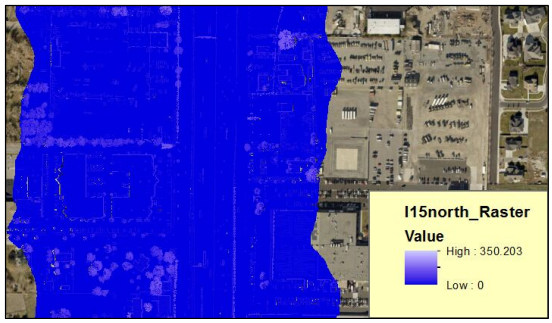

Figure 5.23 Raster Data

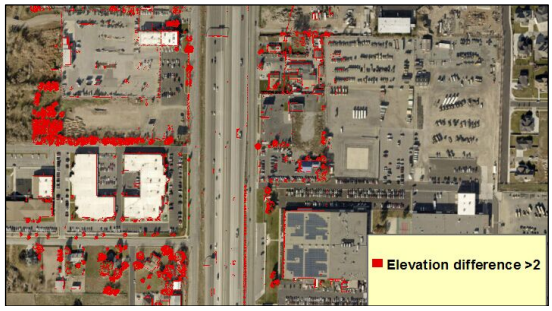

Figure 5.24 Filtered Raster Data

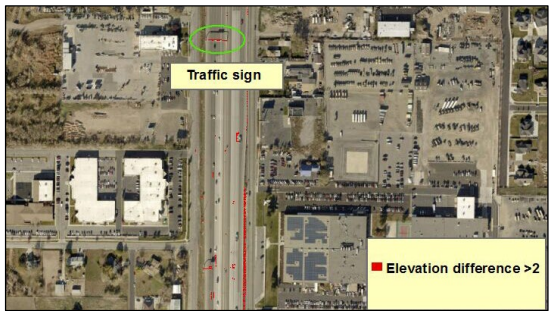

Figure 5.25 Clipped Raster Data

5.3 Road Assets Inventory

With the proposed ArcGIS-based algorithm, we can easily identify different kinds of road assets. However, this algorithm can only help us find road assets. The specific location and structural information of the road assets still need to be collected manually. In this section, we provided our collected information of all the assets that can be identified from airborne LiDAR data and compared them with the Mandli dataset.

5.3.1 I-84

In total, 10 raw airborne LiDAR data files were obtained for the mapping section on I-84: No.1-No.10 (Section 4, Table 4.1). Among them, No. 8 was a duplication of No. 7, and both No. 9 and No. 10 missed some part of the highway. Therefore, in our project, the total valid length of the mapping section was around 15.5 miles, crossing Peterson and Morgan.

With the proposed feature extraction algorithm, we found two overhead traffic signs, 19 light poles, five billboards, and 27 bridges and culverts on the mapping section of I-84. In addition, barriers (excluding

cable barriers) were identified. Figure 5.26 shows all road assets detected on I-84. The geo-location information and structural characteristics of these identified road assets were manually recorded and are provided in Table 1-Table 6 in the Appendix.

5.3.2 US-191

Fourteen raw LiDAR data files were collected for US-191: No. 1-No. 21 (Section 4, Table 4.2). The total effectively mapped highway length was about 28 miles. On the mapping section of US-191, we did not find any recognizable traffic signs, signals, or light poles. We identified one billboard, six bridges and culverts, and all barriers. All road assets we detected on US-191 are shown in Figure 5.27. Detailed geo-location information and structural attributes of these road assets were collected manually and are given in Tables 7-9 in the Appendix.

5.3.3 I-15 North

As introduced in Section 4, I-15 North refers the section from MP 284 to 307 on I-15. In total, 14 raw airborne LiDAR data files were obtained for the mapping section of I-15 North: No. 11-No. 24 (Section 4, Table 4.1). Among them, No. 17 and No. 23 were redundant because their mapping sections were also covered by other LAS data. The total length of the mapping section was around 23 miles.

On I-15 North, we found 192 overhead traffic signs, 178 light poles, 124 billboards, 54 bridges and one culvert on the mapping section of I-15 North. In addition, barriers (excluding cable barriers) were identified using the ArcGIS-based algorithm. Figure 5.28 shows all the road assets we identified on I-15 North. We manually collected the geo-location information and structure characteristics of these identified road assets. Detailed information is given in Tables 10-15 in the Appendix.

5.3.4 I-15 South

On I-15, we also collected airborne LiDAR data from Santaquin to Springville (MP 241 to 260), which is referred to as I-15 south. In total, seven raw airborne LiDAR data files were obtained for the mapping section on I-15 South: No. 25-No. 31 (Section 4, Table 4.1). These LiDAR data were all valid and were used to extract information for the road assets. The total length of the mapping section was around 19 miles.

On I-15 South, 34 overhead traffic signs, 103 light poles, 56 billboards, 33 bridges and four culverts were detected. We also identified all barriers (excluding cable barriers) using the proposed ArcGIS-based algorithm. Figure 5.29 shows all road assets identified on I-15 South. Specific geo-location information and structural attributes about these identified road assets were collected manually. Detailed information is given in Tables 16-21 in the Appendix.

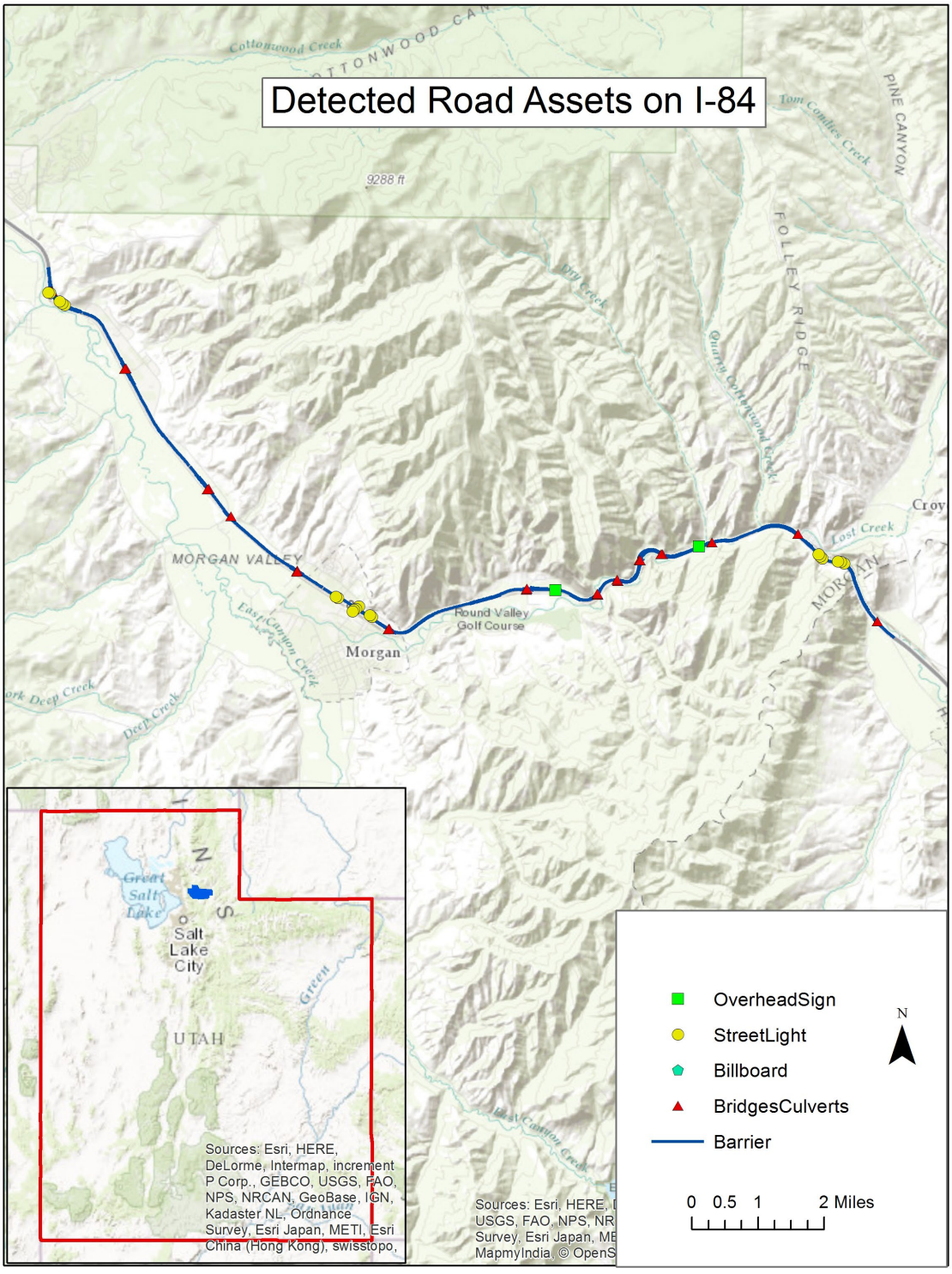

Figure 5.26 Detected Road Assets on I-84

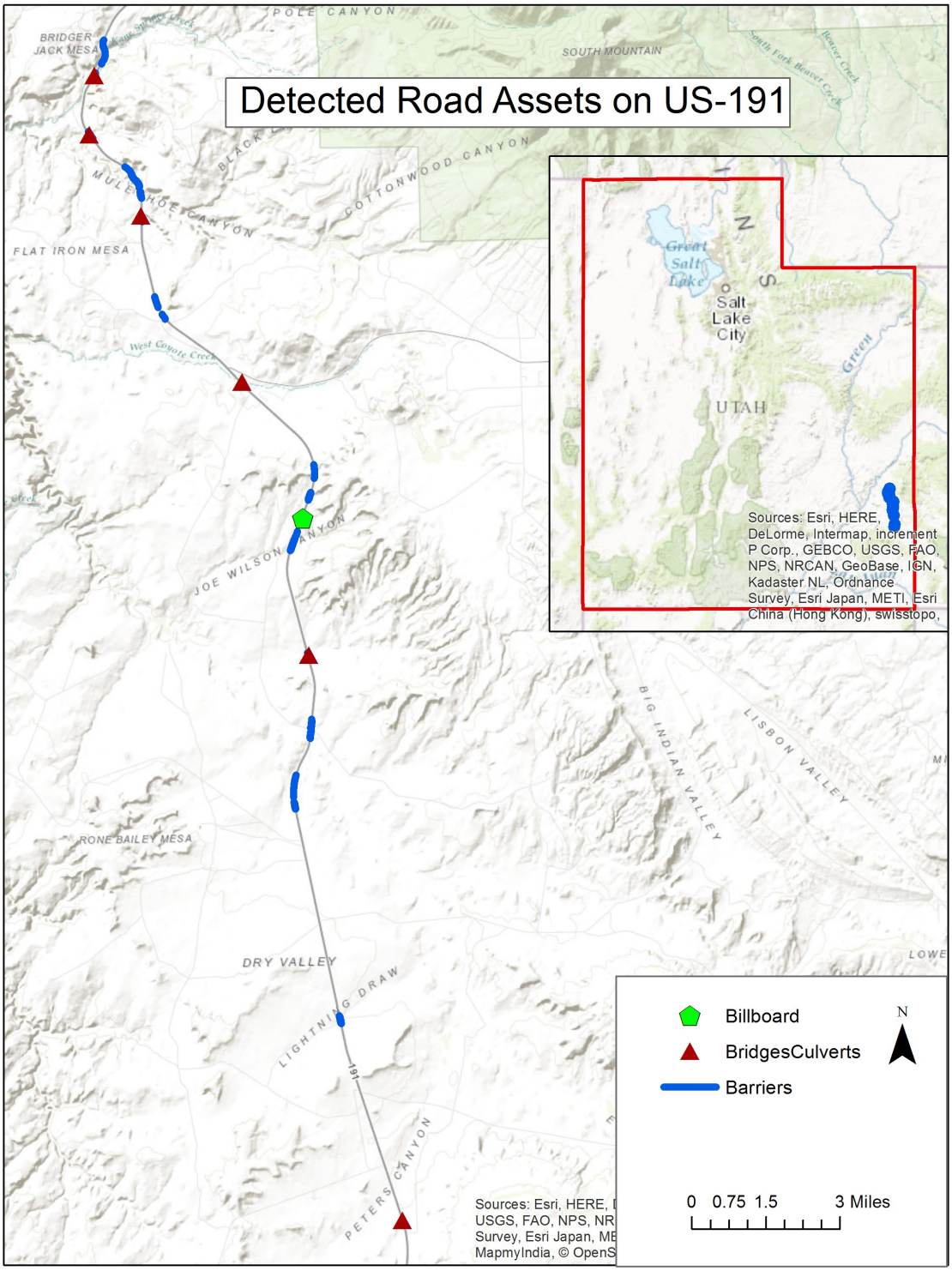

Figure 5.27 Detected Road Assets on US-191

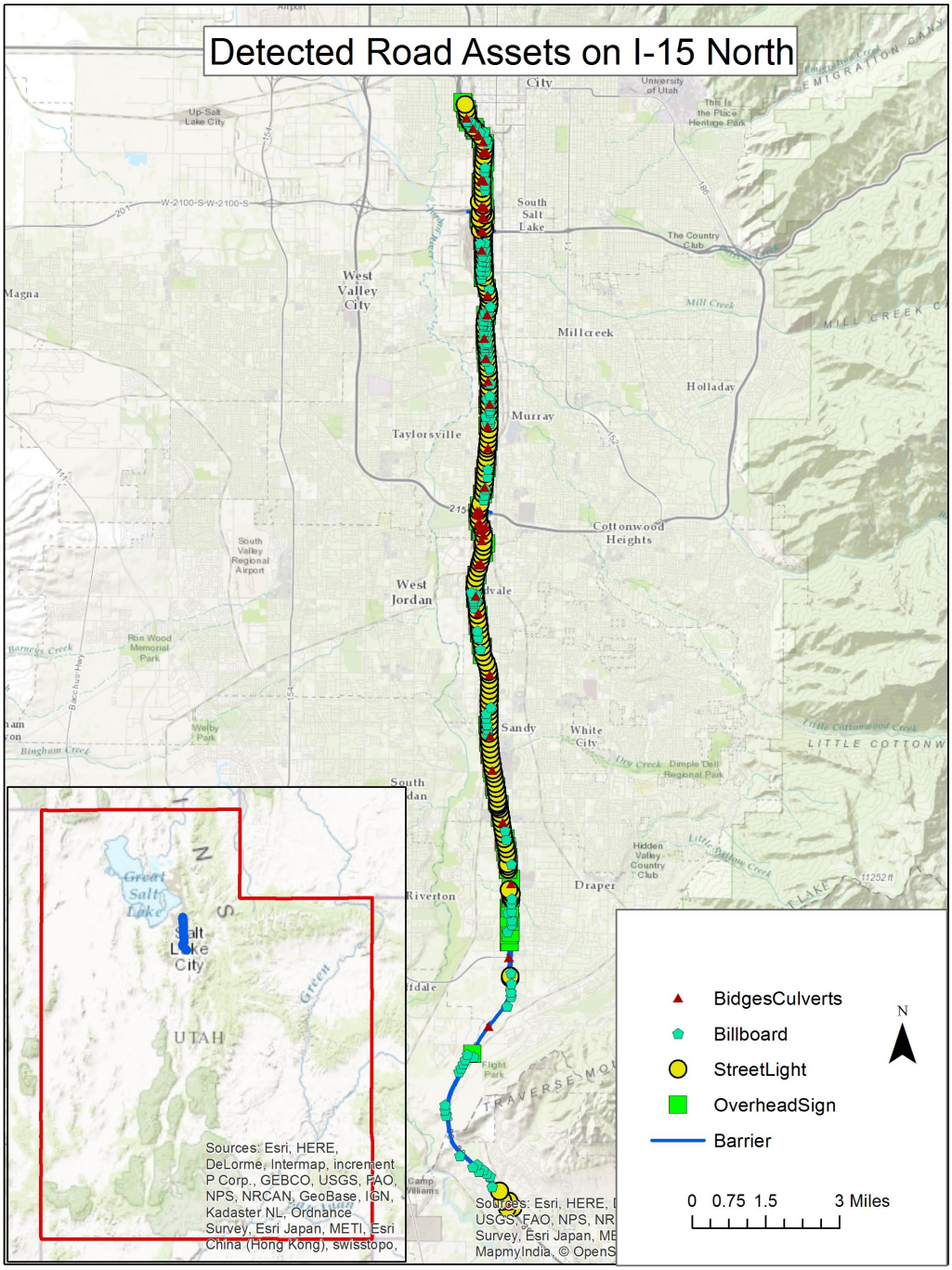

Figure 5.28 Detected Road Assets on I-15 North

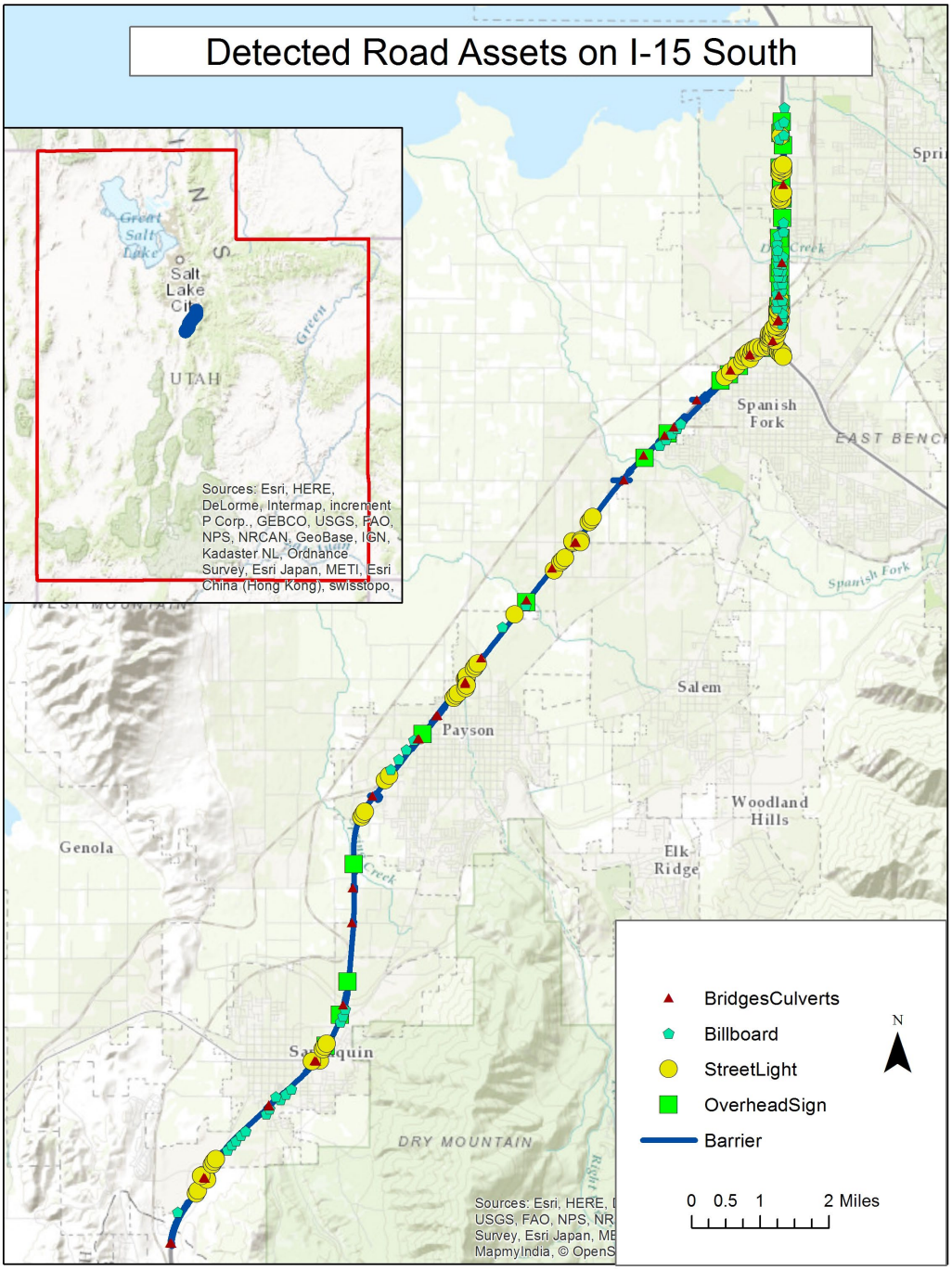

Figure 5.29 Detected Road Assets on I-15 South

5.4 Comparison with Mobile LiDAR

5.4.1 Effectiveness Comparison with Mobile LiDAR

To verify the collected information of road assets from airborne LiDAR data, we compared our results with the existing highway inventory dataset of UDOT, which was collected by Mandli in 2014. The latest Mandli dataset was collect via mobile LiDAR and Photolog imagery. Traffic signs, including small signs and large overhead signs, traffic signals, billboards, and barriers, were all included in the Mandli dataset. Because of the sparseness of the airborne LiDAR points, we could not extract small signs in this research. However, all other assets included in the Mandli dataset were successfully explored. Moreover, we were able to detect bridges and large culverts that cannot be mapped from the mobile platform because of the broad view and different perspective of the aircraft. As shown in Figure 5.30, culverts (a) and bridges (b) are very distinctive in airborne LiDAR data. We also explored the light poles that may be useful to state DOTs but were not detected by Mandli since light poles were not included in the contract. Note that in this study, we only collected the location and size information of assets, the specific contents (e.g., the advertisement details of the billboards, the instruction information of the signs, etc.) with the assets could not be identified. Nevertheless, this kind of information, if deemed important for highway maintenance and asset management, can be easily obtained if we combine LiDAR data with imagery data in the future.

For simplicity, here we used the detection results of billboards as an example to make the comparison. Figure 5.31 shows the comparison between the billboards detected in our research and by Mandli. The billboards in the Mandli dataset are marked with green hexagons, and the billboards detected in our research are marked with black triangles. It can be observed that our detection results match the Mandli dataset well, both in quantity and location.

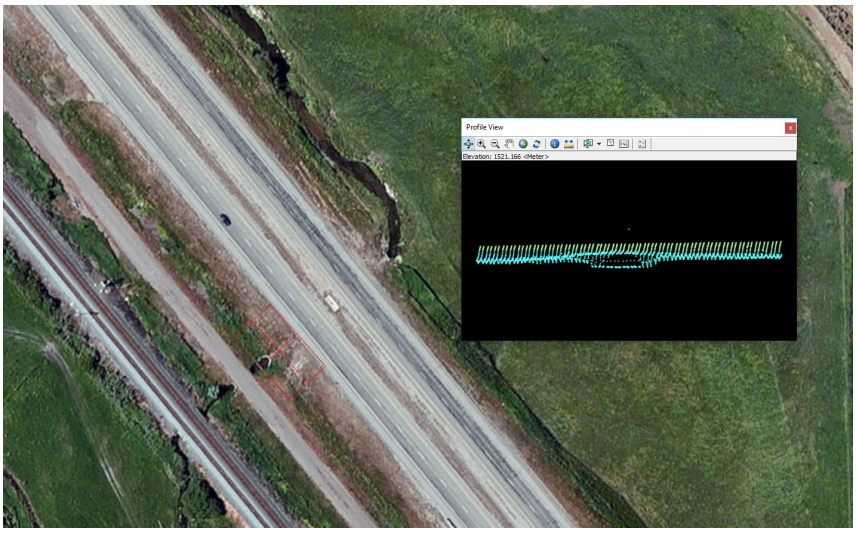

(a)

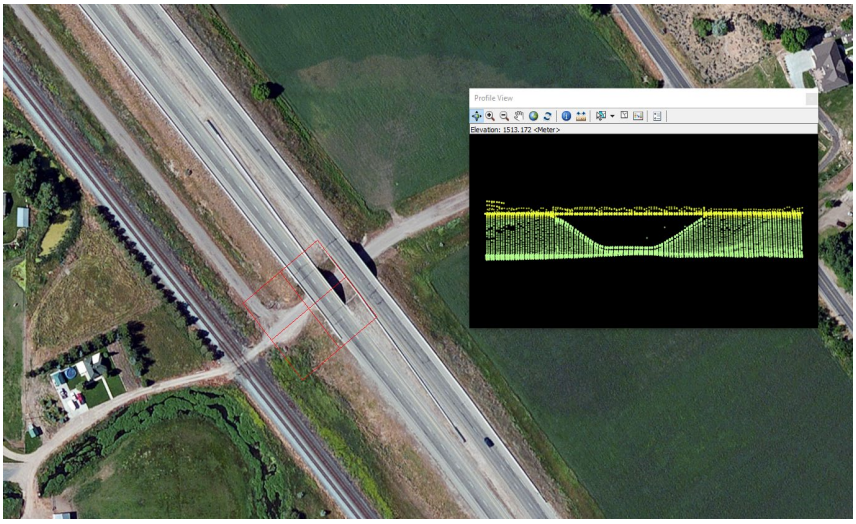

(b)

Figure 5.30 3D View of Culvert and Bridge in Airborne LiDAR Data (a) Culvert (b) Bridge

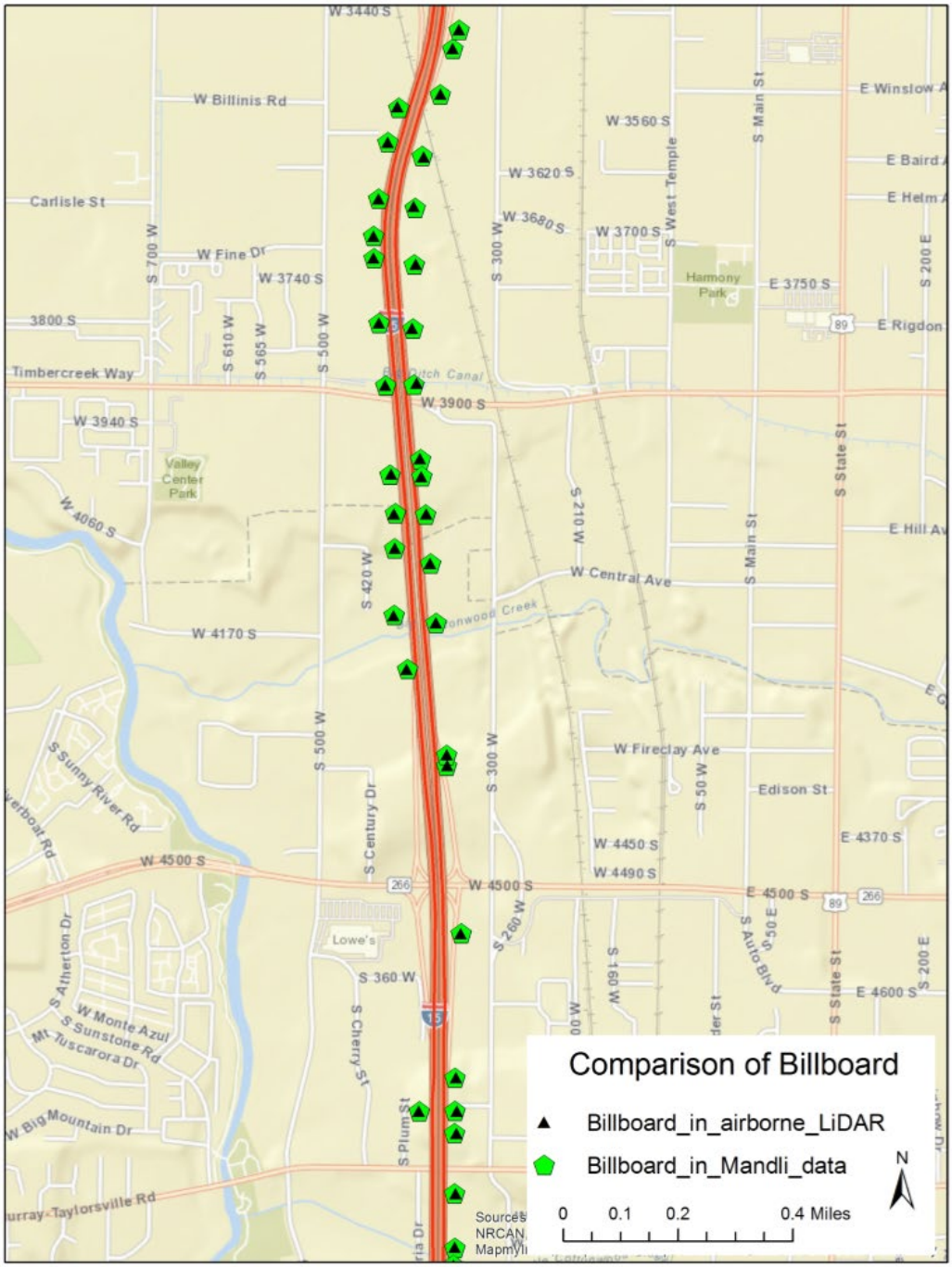

Figure 5.31 Billboards in Mandli Datasets versus Billboards Detected in Our Project

5.4.2 Economic Comparison with Mobile LiDAR

Jayaler et al. (2014) conducted a field experiment to evaluate five highway inventory data collection methods: GPS data logger, robotic total station, GPS enabled photo/video log, satellite/aerial imagery, and mobile LiDAR. They provided a detailed summary about the five methods. The cost and time information of mobile LiDAR were adopted in this paper for comparison purposes. In our study, we did not detect any small signs due to the insufficient point density of airborne LiDAR data. However, small signs could account for a substantial proportion of the total number of assets (about 50% according to the Mandli dataset). Therefore, for fair comparison, we halved the total data reduction time provided by Jayaler et al. (2014) (i.e., the actual total data reduction time of the mobile LiDAR field experiment was 70 man-hours, but was assumed it to be 35 man-hours in this paper). For cost analysis, the unit labor cost in this study is assumed to be the same amount as that adopted by Jayaler et al. (2014): $130 per hour. Regarding the data collection cost, Jayaler et al. (2014) estimated the average cost per mile for mobile LiDAR to be $200, while the total mapping cost of the airborne LiDAR in this study is about $5,000. Note that if a larger area was surveyed with the airborne platform, the unit data collection cost for airborne LiDAR could be even lower due to the economy of scale. Table 5.1 shows the comparison between the mobile LiDAR field trail conducted by Jayaler et al. (2014) and the field experiment in this study.

Based on Table 5.1, the data collection efficiency of airborne LiDAR is much higher than mobile LiDAR. The difference in data reduction speed between the two methods demonstrates that the proposed ArcGIS-based algorithm can reduce the data reduction time to some extent. Furthermore, the average cost per mile for airborne LiDAR and mobile LiDAR methods are $292.1 and $590.0, respectively. Thus, we can conclude that the airborne LiDAR method is more economical than mobile LiDAR in highway asset inventory.

Table 5.1 Economic Comparison Between Airborne LiDAR and Mobile LiDAR

Methods	Total mapping length (mi)	Total data collection time (man-hr)	Total data reduction time (man-hr)	Data collection cost ($/mi)	Labor cost ($/man-hr)	Average time (man-hr/mi)	Average cost ($/mi)
Mobile LiDAR	14.2	8.0	35.0	200.0	130.0	3.0	590.0
Airborne LiDAR	86.0	4.8	150.0	58.1	130.0	1.8	292.1

6. DRAINAGE GRATE DETECTION USING MATLAB

This section presents an automatic highway drainage grate detection and recognition algorithm based on aerial images. Drainage systems that remove storm water from highways are very important factors for maintaining highway safety. The statistics of drainage assets on highway systems are essential for state DOTs or local agencies to manage and upgrade drainage features. However, the significant number of these drainage grates along U.S. highways can make their manual detection and analysis laborious. To address these challenges, this section proposes a method to directly extract drainage grates from aerial photos of highways.

Drainage grates, unlike traffic signs that are brightly painted and particularly shaped, usually have a dark color and small size, making them hard to recognize in ground-based photos or videos. But aerial images obtained from flights can clearly show the shape and color of drainage grates (Figure 6.1). Thus, in this section, our goal is to formulate a general framework of detecting and recognizing highway drainage grates based on aerial image processing.

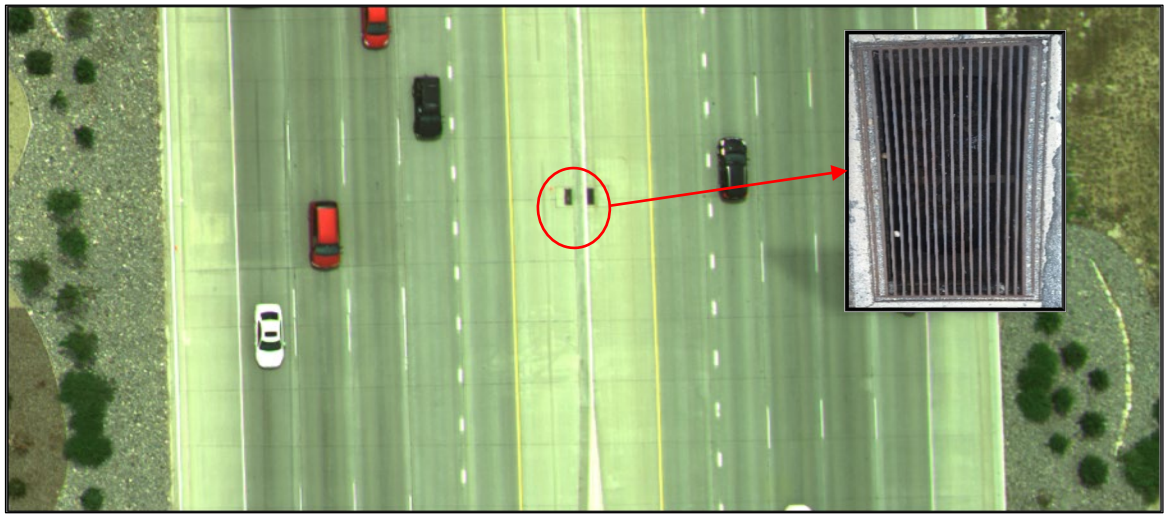

Figure 6.1 Drainage Grates from an Aerial Image

Figure 6.2 shows the flowchart of the algorithm for drainage grate detection.

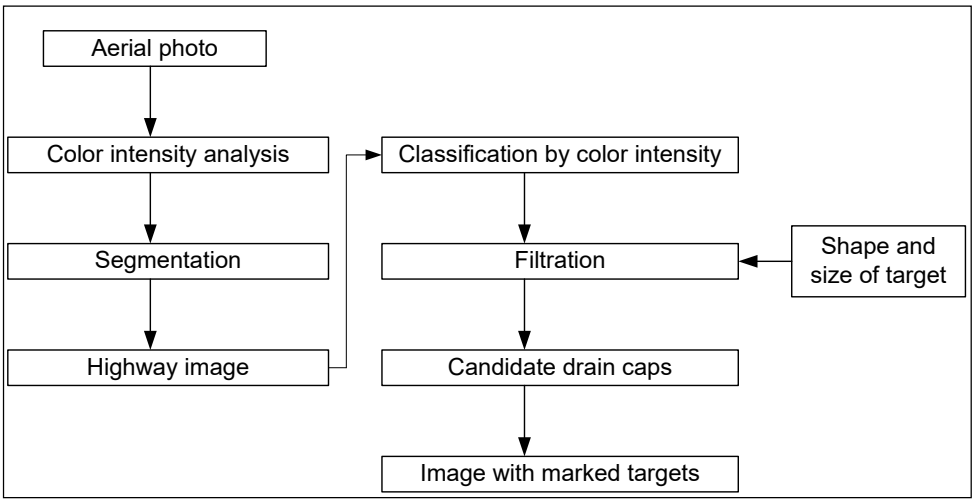

Figure 6.2 Drainage Grate Detection Flowchart

6.1 Road Segmentation

For the drainage grates on the highway, the main features that can distinguish them are their dark color and rectangular shape. However, other objects in the image also have either a similar color or shape. Within the highway surface, the main objects similar to the drainage grates are the windshields of white cars. Outside the highway surface, the shrubs or other objects may have a similar dark color as the drainage grates. In order to eliminate the interference of the bare ground and shrubs, we first extracted the highway surface from the aerial images. As we can see in Figure 6.1, the highway surface has a relatively light color compared with the color of the bare ground or shrubs. Based on this characteristic, we can roughly divide the image into two parts, where the light-colored part should be the highway surface and the dark-colored part will be the bare ground and shrubs.

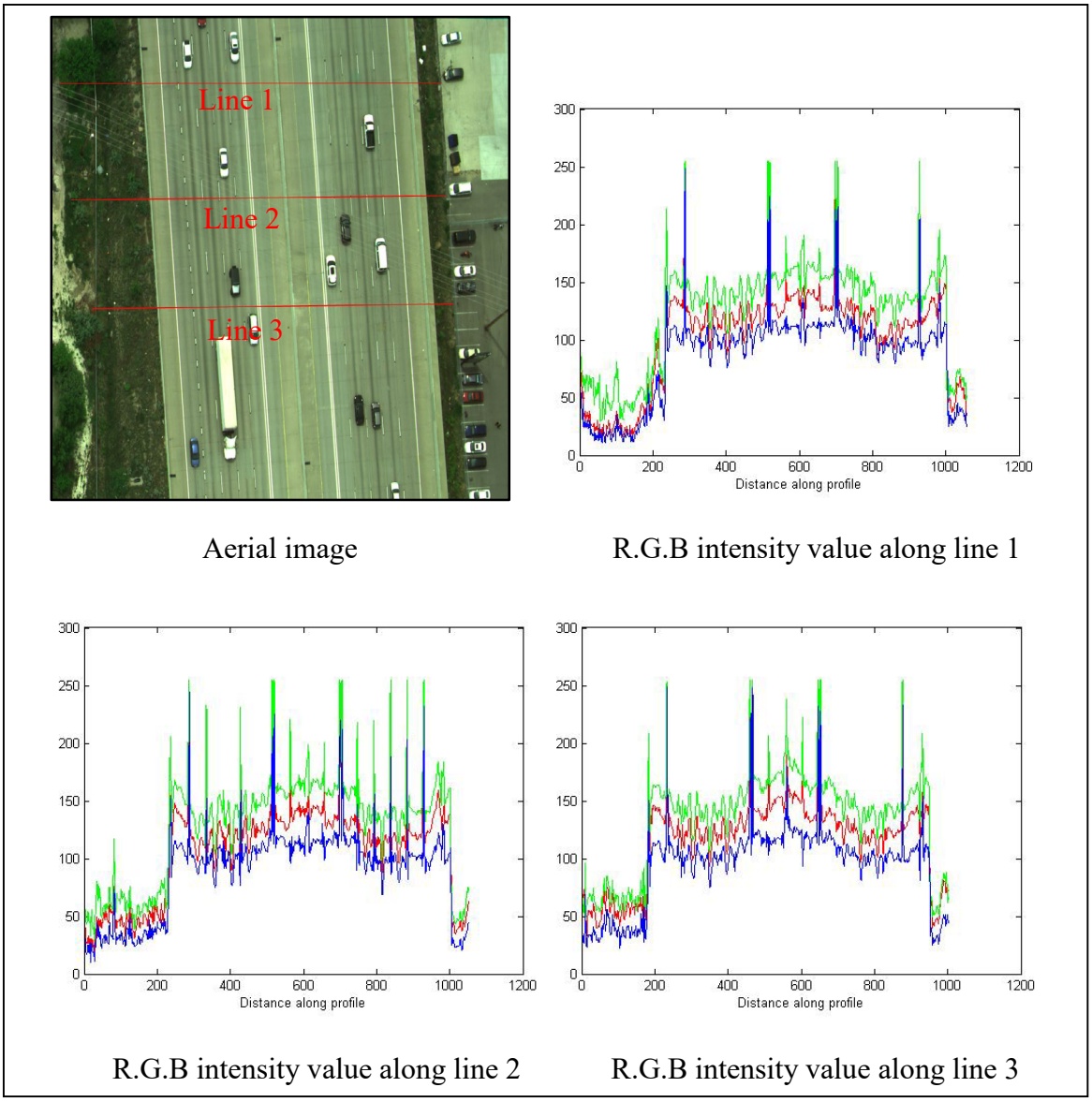

Aerial image

R.G.B intensity value along line 1

R.G.B intensity value along line 2

R.G.B intensity value along line 3

Figure 6.3 Road Surface Color Characteristic Analysis

In order to get an appropriate demarcation, we first analyzed the color distribution within the image. As shown in Figure 6.3, we chose several profiles of the highway and analyzed the color composition of each pixel along the profile. We can observe that, approximately, the intensity values of red, green, and blue of pixels representing the highway surface are all larger than the values of pixels representing bare ground or shrubs.

Obviously, for each pixel, the intensity values for R, G, and B colors have the same trend. If the intensity level of red for one pixel is high, the intensity level of green and blue for that pixel will also be high, and vice versa. From Figure 6.3, we can observe that the intensity value of pixels that represent ground or shrubs falls into the 0-100 range, while road surface falls into the 80-180 range. In order to make the difference (between highway surface and ground) more significant, we sum up the intensity values of red, green, and blue for each pixel and assign the value to the corresponding pixel, resulting in a new matrix, I (Figure 6.4).

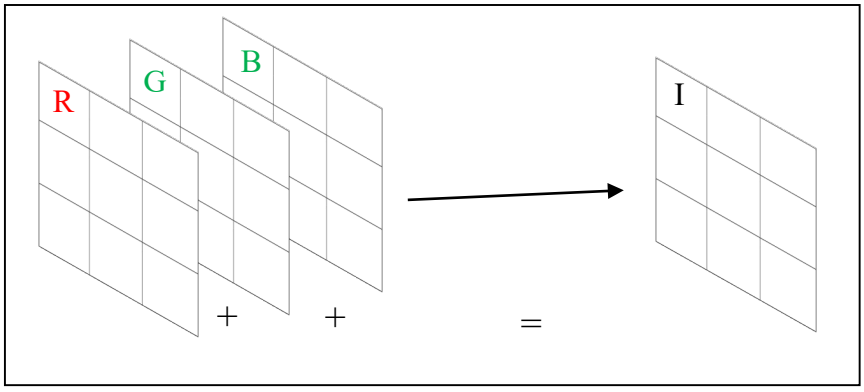

Figure 6.4 Summation of R, G, B Color Band

$$I(i,j) = R(i,j) + G(i,j) + B(i,j) \qquad \forall\, i \in [1,M], j \in [1,N] \tag{9}$$

$$I(i,j) = 1 \qquad \forall I(i,j) \geq T_1 \tag{10}$$

$$I(i,j) = 0 \qquad \forall I(i,j) \leq T_1 \tag{11}$$

where I is the summation value, M is the number of columns in the image, N is the number of rows in the image, and T_1 is the threshold value that determines the boundary of the road and non-road. In this project, we use $T_1 = 300$.

We assigned 0 to pixels with values smaller than 300 and 1 to pixels with values larger than 300. Figure 6.5 is the original image. After using the thresholding method, the resulting image is shown in Figure 6.6, where white pixels have a value of 1 and black pixels have a value of 0. Note that within the range of highway surface, pixels representing dark-colored objects were assigned a value of 0; whereas, outside the range of the highway surface, some objects, such as parking lots and light-colored roofs, are misclassified as highway. Thus, the morphological opening and closing as well as BoundingBox methodologies were used to eliminate the misclassified data. Figure 6.7 shows the resulting image. Finally, the non-highway part was deleted from the original image.

Figure 6.5 Original Image

Figure 6.6 Thresholded Image

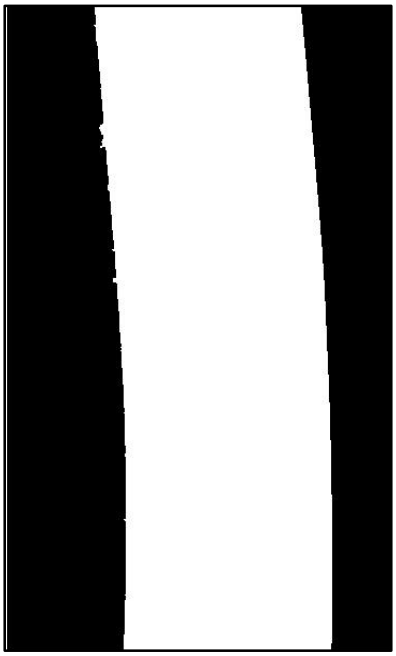

Figure 6.7 Road Surface

6.2 Drainage Grate Detection

6.2.1 Color Thresholding

After segmenting the highway surface from the image, our next step was to extract the drainage grates. As with the road extraction, we also used color characteristics to detect the drainage grates because their color is quite different from the highway surface color. We still used the profile analysis method to evaluate the intensity value of the drainage grates. Figure 6.8 shows the results of three profiles displaying the contradistinction between the intensity values of drainage grates and highway surface. It is fairly clear that the intensity values for all R, G, and B bands for the drainage grates were no greater than 80 in most cases. Similarly, we summed up the intensity values of red, green, and blue colors for each pixel and assigned the value to the corresponding pixel, then used the threshold value of $240 = 3 \times 80$ to classify the image.

$$I(i,j) = 1 \qquad \forall I(i,j) \leq T_2 \tag{12}$$

$$I(i,j) = 0 \qquad \forall I(i,j) \geq T_2 \tag{13}$$

where $T_2 = 240$.

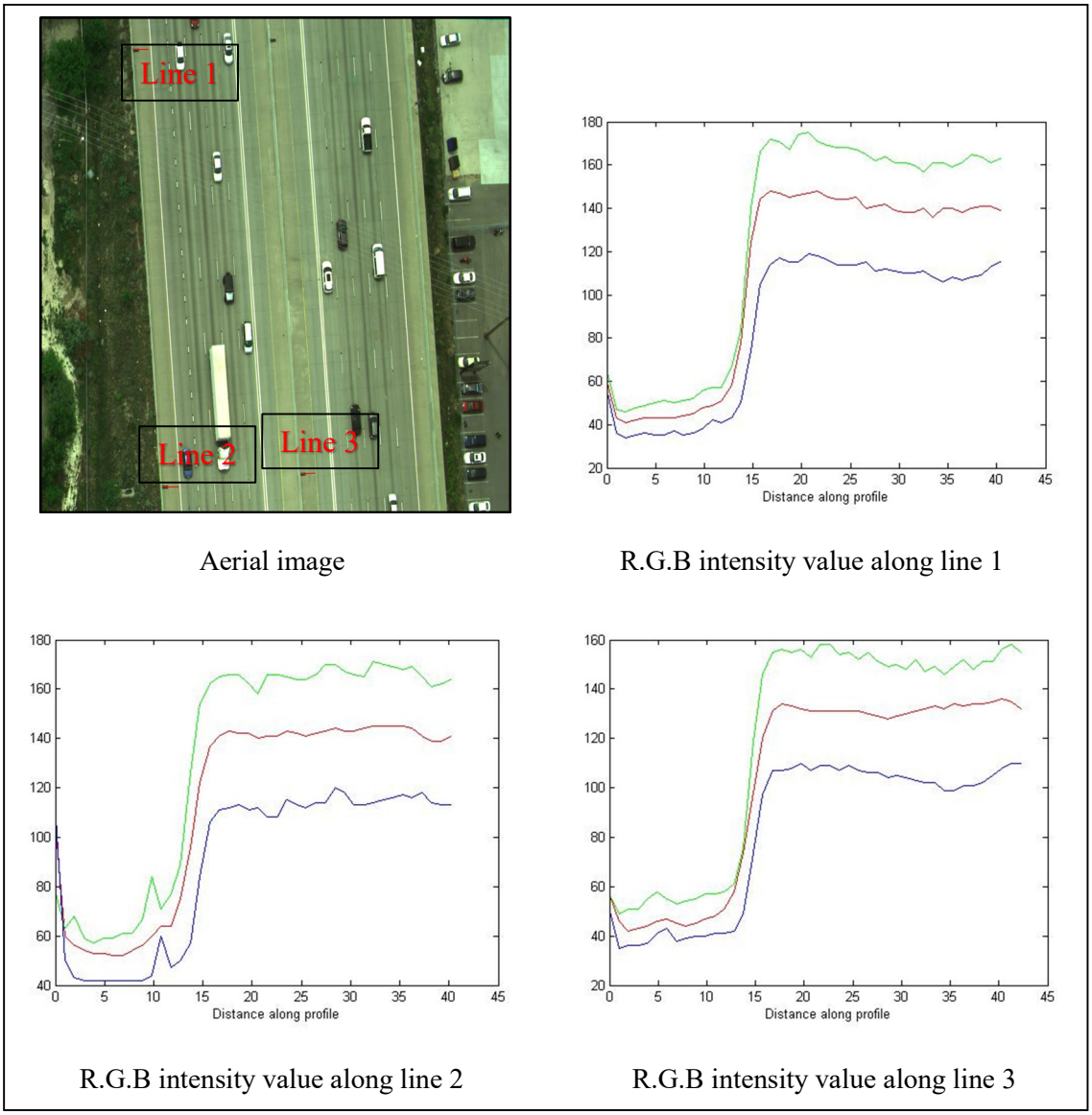

Aerial image

R.G.B intensity value along line 1

R.G.B intensity value along line 2

R.G.B intensity value along line 3

Figure 6.8 Drainage Grate Color Characteristic Analysis

6.2.2 Shape Analysis

We can observe from the original aerial image that black cars or the windshields of white cars have a similar color as the drainage grates. Thus, using only color thresholding is not enough to get the ideal extraction results. Therefore, we used shape characteristics for further analysis. The previously discussed results of color thresholding will be the image with a series of connected components that represent the drainage grates, black cars, windshields, or other objects. Each connected component has its own shape and area. The shape of the connected components that represent the drainage grates is nearly rectangular, and size is also relatively unified. For the purpose of evaluating the property of the drainage grates, we measured the length, width, and area of 31 connected components that we preliminarily determined to be drainage grates. Table 6.1 shows the statistical values of the 31 connected components.

Table 6.1 Statistics of the Chosen Samples

Number	**1**	**2**	**3**	**4**	**5**	**6**	**7**	**8**	**9**	**10**	**11**	**12**	**13**	**14**	**15**	**16**
Length	14	16	15	13	14	14	14	15	13	14	13	13	14	11	5	14
Width	7	7	8	8	5	6	5	6	5	7	6	7	6	5	13	5
Area	81	84	87	83	58	75	62	81	60	83	71	84	81	52	60	63
Number	**17**	**18**	**19**	**20**	**21**	**22**	**23**	**24**	**25**	**26**	**27**	**28**	**29**	**30**	**31**	
Length	14	15	14	15	13	15	15	14	15	7	15	6	7	13	6	
Width	9	8	7	8	8	6	8	8	7	15	7	14	14	6	14	
Area	110	102	84	94	97	79	88	83	91	86	87	75	84	67	77	

Based on the data in Table 6.1, length ranged from 5 to 16, width ranged from 5 to 15, and area ranged from 52 to 110. We set the lower and upper limits of length and width to 5 and 20, respectively, and the threshold values of area were set to 30 and 150 to cover more cases. The connected components that satisfy the following constraints were regarded as candidate drainage grates.

$$T_2 \leq L(k) \leq T_3 \tag{14}$$

$$T_2 \leq W(k) \leq T_3 \tag{15}$$

$$L(k) + W(k) \leq T_4 \tag{16}$$

$$|L(k) - W(k)| \geq T_5 \tag{17}$$

$$T_6 \leq \mathrm{A}(k) \leq T_7 \tag{18}$$

where $L(k)$, $W(k)$, and $\mathrm{A}(k)$ are the length, width, and area of the kth connected component, respectively, and $T_2 = 5, T_3 = 20, T_4 = 30, T_5 = 5, T_6 = 3$, and $T_7 = 150$. For each connected component, constraints (14) and (15) restricted the range of length and width while constraint (16) limited the area. Constraints (17) and (18) further restricted the shape of the connected components to be approximately rectangular.

6.2.3 Filtration

Shape analysis can help us eliminate the interference of dark-colored cars while the windshields of white cars, whose color and shape are both similar to the drainage grates, cannot be completely removed. Hence, we used the following procedure to further filtrate the drainage grates:

- Use color thresholding to identify white cars, excluding the windshield.
- Use morphological operation to get the entire range of cars.
- Remove all candidate connected components that fall into the range of cars.

Figure 6.9 is the original image. Figure 6.10 shows an example of the detection results; the drainage grates are marked by blue crosses.

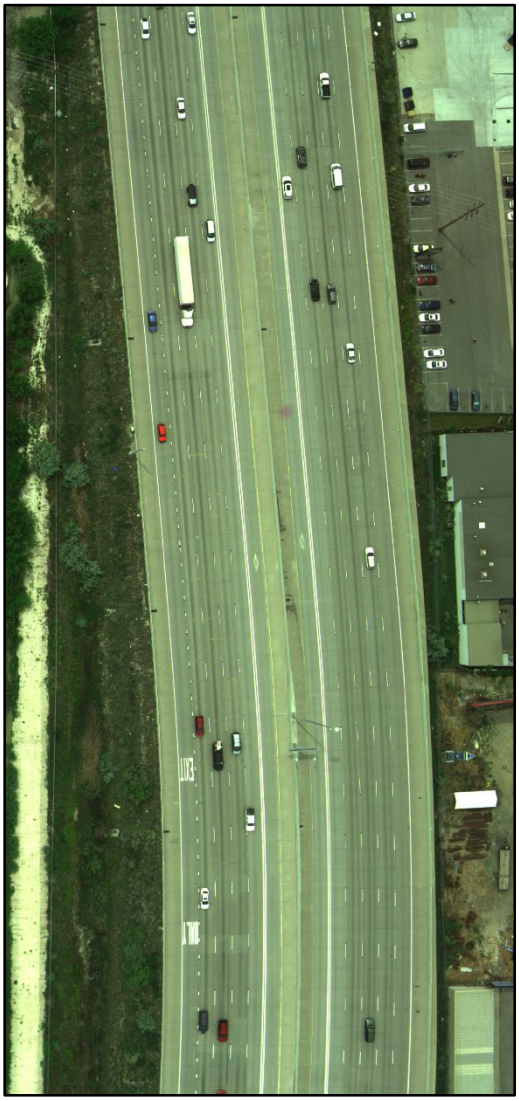

Figure 6.9 Original Image

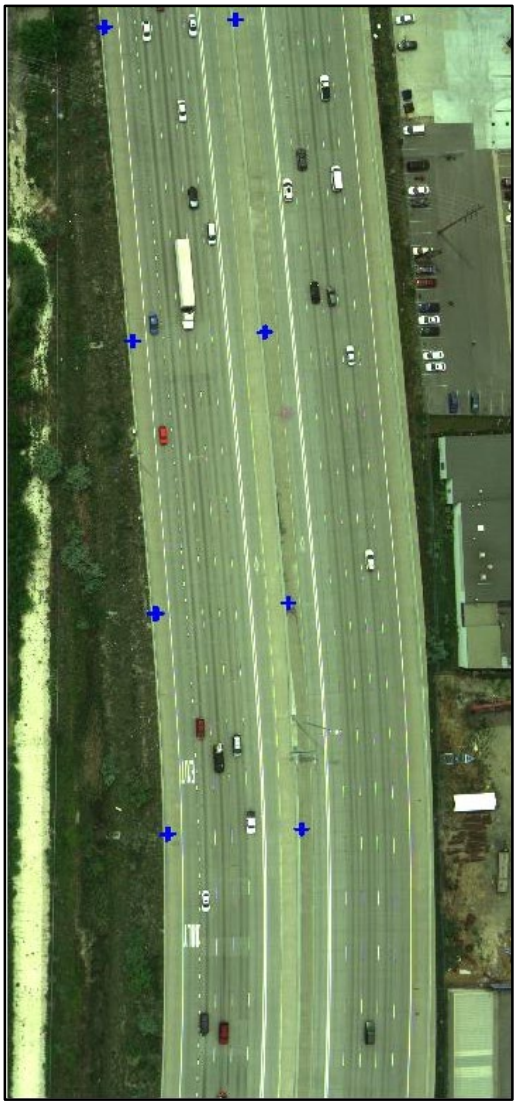

Figure 6.10 Detection Result

6.3 Results and Conclusion

The algorithm was tested on 20 images, and the results are given in Table 6.2. In the evaluation table, True Positive (TP) means that the drainage grate was correctly detected, True Negative (TN) means that the drainage grate was missed, and False Positive (FP) means that the object was not a drainage grate but was detected as a drainage grate. Actual Number (AN) is the number of drainage grates counted manually, which is the summation of TP and Missed TN. AN is considered as accurate in our study. Completeness is the completion rate, and Correctness is the right detection rate.

$$AN = TP + TN \tag{19}$$

$$Completeness = \frac{TP}{AN} \tag{20}$$

$$Correctness = \frac{TP}{TP + TN + FP} \tag{21}$$

According to the data in Table 6.2, the completeness of the algorithm on the 20 testing images is 89.3% while correctness is 77.9%. For some images, we can see that both completeness and correctness are high; for other images, the algorithm does not work well. The quality of images and road segmentation are the main factors influencing the performance of our algorithm. To further improve the image quality, we should collect data on fair-weather days and fly the plane at a lower altitude. In addition, in our algorithm, the parameters used to filtrate drainage grates are adjustable. If we choose those parameters that can eliminate more interference objects similar to drainage grates, some drainage grates that are less legible may also be eliminated; if we try to detect all the drainage grates, even those that are irregular or illegible, more interference objects will be misidentified as drainage grates. In the future, we should focus on the improvement of the road segmentation method and the refinement of our algorithm to make it more robust.

Table 6.2 Drainage Grate Detection Results and Accuracy Evaluation

	Detection Results				**Accuracy Evaluations**	
Image Number	True Positive	True Negative	False Positive	Actual Number	Complete-ness (%)	Correct-ness (%)
1	17	0	1	17	100	94.4
2	8	0	0	8	100	100
3	10	0	1	10	100	90.9
4	12	1	1	13	92.3	85.7
5	9	2	3	11	81.8	64.3
6	8	0	3	8	100	72.7
7	14	2	5	16	87.5	66.7
8	10	5	1	15	66.7	62.5
9	16	4	2	20	80	72.7
10	4	2	1	6	66.7	57.1
11	11	0	1	11	100	91.7
12	14	2	4	16	87.5	70
13	15	4	2	19	78.9	71.4
14	20	0	1	20	100	95.2
15	17	2	3	19	89.5	77.3
16	18	0	2	18	100	90
17	8	0	1	8	100	88.9
18	18	3	2	21	85.7	78.3
19	10	2	7	12	83.3	52.6
20	19	2	1	21	90.5	86.4
Total	258	31	42	289	89.3	77.9

7. CONCLUSION AND FUTURE WORK

Highway inventory data collection is a complicated and repetitive task that requires a lot of labor and resources. State DOTs and transportation agencies are always looking for better techniques to reduce costs. Currently, the commonly used techniques include field inventory, photo/video log, integrated GPS/GIS mapping systems, aerial/satellite photography, terrestrial LiDAR, mobile LiDAR, and airborne LiDAR. Among them, the air-based methods, namely, aerial/satellite photography and airborne LiDAR, are less popular. The concerns about the low accuracy and high cost of air-based methods are the main reasons that hinder their application in highway feature inventory.

We conducted field data collection along several highway segments in Utah. Four highway sections were mapped: I-15 North, I-15 South, I-84, and US-191, covering approximately 86 miles of highway in total. Based on the collected data, we analyzed and reported the accuracy of the data and compared it with the required accuracy standard from USGS. The results showed that the accuracy of the collected data generally meets the requirements.

To verify the economic efficiency of airborne data collection methods, we compared the cost of our field data collection with a mobile-based data collection reported by Jayaler et al. (2014). We found that, although the fixed cost and the hourly cost of airborne data collection are higher than the mobile-based method, the average data collection cost per mile of the airborne method is less than the mobile-based method due to the much higher mapping speed of aircraft. Thus, for large mapping areas, the airborne data collection method is more economical than the mobile-based method.

Although we can efficiently map highways using aircraft, the process of extracting highway features from airborne data is time consuming and labor intensive. The advantage of efficient data collection of airborne method would be compromised if the feature extraction process can only be completed manually. Therefore, we proposed an ArcGIS-based algorithm and a MATLAB-based algorithm to efficiently extract highway features from airborne LiDAR data and aerial imagery data, respectively. We processed all the valid LiDAR data and some of the high-quality images using our algorithms. The experimental results demonstrated the feasibility of our proposed algorithms in detecting certain types of highway features (e.g., barriers, traffic signs, bridges, large culverts, and drainage grates). We also compared the efficiency and the cost of the feature extraction in our experiment with that reported by Jayaler et al. (2014). The results showed, with the proposed algorithm, we could achieve higher feature extraction efficiency than that reported by Jayaler et al. (2014).

In the process of highway feature extraction, we successfully identified large traffic signs, large traffic signals, bridges, large culverts, light poles, billboards, and barriers from the airborne LiDAR data and extracted drainage grates from aerial imagery data. However, due to the limited point density and the overhead view of airborne LiDAR data, small traffic signs, small traffic signals, and cable barriers can hardly be identified in the collected airborne LiDAR data. Nevertheless, the drawback of missing small targets from airborne LiDAR data could be alleviated by repeating the mapping process, lowering flight altitude, and slowing flight speed. With the development of LiDAR technology, the scanning frequency of LiDAR sensors may also be improved significantly in the near future. Furthermore, this disadvantage could also be compensated by combining air-based data collection methods with other data collection techniques (e.g., mobile-based method or manual inventory). On the other hand, airborne LiDAR has the advantage over ground-based inventory technologies of being able to provide a different perspective. As a result, it can detect objects, such as culverts and ditches, which may have been hidden from the mobile platform. Therefore, airborne LiDAR is a promising technique that can serve as a complement to other techniques for road inventory data collection.

Based on the results of this research, we can conclude that with currently available technologies, airborne data collection could reach required data accuracy. In addition, for large mapping areas, an airborne data collection method could be more efficient in terms of both time and expense. Hence, when creating or updating a statewide database of highway assets, airborne data collection methods are competitive alternatives.

In summary, we investigated the applicability of airborne data collection methods, including the airborne LiDAR technique and aerial photography method, for collecting highway inventory data. The main contributions of this research include the following:

- Airborne data collection methods were used to map several highway segments in Utah.
- The accuracy and the cost of airborne data collection methods were analyzed and reported.
- An ArcGIS-based algorithm and a MATLAB-based algorithm were proposed to efficiently extract highway features from airborne LiDAR data and aerial imagery data, respectively.
- We developed a shape file for each mapping section, which can be directly added to the UDOT database.
- Based on the application results, we analyzed the advantages and disadvantages of using airborne data collection methods in highway inventory and provided some guidelines for future studies and applications.

A number of research extensions can be considered in future studies. First, the ArcGIS-based algorithm we proposed is semi-automatic; we plan to develop a program to make it fully automatic. Second, we will combine the LiDAR data with imagery data to improve detection accuracy and develop new methods to detect some additional features.

8. REFERENCES

Balali, V., Golparvar-Fard, M., 2015. "Evaluation of multiclass traffic sign detection and classification methods for US roadway asset inventory management." *Journal of Computing in Civil Engineering*, *30*(2), 04015022.

Baltsavias, E. P., 1999. Airborne laser scanning: existing systems and firms and other resources." *ISPRS Journal of Photogrammetry and Remote sensing*, *54*(2-3), 164-198.

Bernardini, F., Sgambati, A., Kokelj, M. M., Zaccaria, C., Micheli, R., Fragiacomo, A., De Min, A., 2013. "Airborne LiDAR application to karstic areas: the example of Trieste province (north-eastern Italy) from prehistoric sites to Roman forts." *Journal of Archaeological Science*, *40*(4), 2152-2160.

Chen, Q., Laurin, G. V., Battles, J. J., Saah, D., 2012. "Integration of airborne lidar and vegetation types derived from aerial photography for mapping aboveground live biomass." *Remote Sensing of Environment*, *121*, 108-117.

DeGray, J., Hancock, K. L., 2002. *Ground-based image and data acquisition systems for roadway inventories in New England: A synthesis of highway practice* (No. NETCR 30,). New England Transportation Consortium.

Doneus, M., Doneus, N., Briese, C., Pregesbauer, M., Mandlburger, G., Verhoeven, G., 2013. "Airborne laser bathymetry–detecting and recording submerged archaeological sites from the air." *Journal of Archaeological Science*, *40*(4), 2136-2151.

Garcia, M. A., Sotelo, M. A., Gorostiza, E. M. 2003. Traffic sign detection in static images using matlab. In Emerging Technologies and Factory Automation, 2, 212-215.

Goyer, G. G., Watson, R., 1963. "The laser and its application to meteorology." *Bulletin of the American Meteorological Society*, *44*(9), 564-570.

Grejner-Brzezinska, D. A., 2005. *Airborne LiDAR: a new source of traffic flow data, research implementation plan* (No. FHWA/OH-2005/14). Ohio State University. Center for Mapping.

Hallmark, S. L., Veneziano, D. A., Souleyrette, R. R., 2001. Evaluating remotely sensed images for use in inventorying roadway infrastructure features.

Highway Safety Manual, 2010. American of State Highway and Transportation Officials.

He, Y., 2016. An analysis of airborne data collection methods for updating highway feature inventory. Utah State University.

He, Y., Song, Z., Liu, Z., Lindsey, R., 2016. Implementation of Aerial LiDAR Technology to Update Highway Feature Inventory (No. UT-17.06).

He, Y., Song, Z., Liu, Z., 2017a. Updating highway asset inventory using airborne LiDAR. Measurement, 104, 132-141.

He, Y., Song, Z., Liu, Z., Heaslip, K., 2017b. Highway Drainage Grate Detection and Recognition Based on Aerial Image Processing (No. 17-04074).

Hill, J. M., Graham, L. A., Henry, R. J., Cotter, D. M., Young, D., 2000. "Wide-area topographic mapping and applications using airborne light detection and ranging (LIDAR) technology." *Photogrammetric Engineering and Remote Sensing*, *66*(8), 908-960.

Jalayer, M., Zhou, H.; Gong, J., Hu, S., and Grinter, M., 2014. "A comprehensive assessment of highway inventory data collection methods." *Journal of the Transportation Research Forum*, Vol 53, No. 2, pp. 73-92.

Jalayer, M., Hu, S., Zhou, H., and Turochy, R. E., 2015. Evaluation of Geo-Tagged Photo and Video Logging Methods to Collect Geospatial Highway Inventory Data. Papers in Applied Geography, Vol. 1, No. 1, pp. 50-58.

Jeyapalan, K., 2004. "Mobile digital cameras for as-built surveys of roadside features." *Photogrammetric Engineering & Remote Sensing*. Vol. 79, No. 3, pp. 301-312.

Jeyapalan, K., Jaselskis, E., 2002. *Technology transfer of as-built and preliminary surveys using GPS, soft photogrammetry, and video logging* (No. Iowa DOT Project TR-446,).

Jeyapalan, K., Bhagawati, D., 2000. "As built surveys of road side features for GIS, visualization, and virtual reality." *International Archives of Photogrammetry and Remote Sensing*, *33*(B5/1; PART 5), 406-413.

Khattak, A. J., Hummer, J. E., Karimi, H. A., 2000. "New and existing roadway inventory data acquisition methods." *Journal of Transportation and Statistics*, *3*(3), 33-46.

Landa, J., and Prochazka, D., 2014. "Automatic road inventory using LiDAR." *Procedia Economics and Finance*, Vol 12, pp. 363-370.

Sallah, S. S. M., Hussin, F. A., Yusoff, M. Z., 2010, June. "Shape-based road sign detection and recognition for embedded application using matlab." In *Intelligent and Advanced Systems (ICIAS), 2010 International Conference on* (pp. 1-5). IEEE.

Sakthivel, K., Nallusamy, R., Kavitha, C., 2015. "Color Image Segmentation Using SVM Pixel Classification Image." *World Academy of Science, Engineering and Technology, International Journal of Computer, Electrical, Automation, Control and Information Engineering*, *8*(10), 1919-1925.

Tao, C.V., 2000. "Mobile mapping technology for road network data acquisition." *Journal of Geospatial Engineering*, Vol. 2, No. 2, pp. 1-14.

Uddin, W., 2008. "Airborne laser terrain mapping for expediting highway projects: Evaluation of accuracy and cost." *Journal of Construction Engineering and Management*, Vol. 136, No. 6, pp. 411-420.

Uddin, W., Al-Turk, E., 2001, August. Airborne LIDAR digital terrain mapping for transportation infrastructure asset management. In *Proceedings, Fifth International Conference on Managing Pavements* (pp. 11-14).

Vosselman, G., Maas, H. G., 2010. *Airborne and terrestrial laser scanning*. CRC.

Wehr, A., Lohr, U., 1999. "Airborne laser scanning—an introduction and overview." *ISPRS Journal of photogrammetry and remote sensing*, *54*(2-3), 68-82.

Williams, K., Olsen, M. J., Roe, G. V., Glennie, C., 2013. "Synthesis of transportation applications of mobile LiDAR." *Remote Sensing*, *5*(9), 4652-4692.

Zhao, L., Lai, Z., Li, Y., Xue, Y., Liao, M., Wu, Z., Liu, P., Liu, X., 2008. "Application and analysis of airborne LiDAR technology in topographic survey of tidal flat and coastal zone." *The International Archives of the Photogrammetry, Remote Sensing and Spatial Information Sciences*. Vol. XXXVII, Part B3b.

Zhou, H., Jalayer, M., Gong, J., Hu, S., Grinter, M., 2013. *Investigation of methods and approaches for collecting and recording highway inventory data.*